INVESTIGATION OF THE ADSORPTION BEHAVIOR OF CESIUM, BARIUM AND PHENOL ONTO MODIFIED HUMIC ACID AND IRON NANOPARTICLES

A THESIS

SUBMITTED TO THE DEPARTMENT OF CHEMISTRY

AND THE INSTITUTE OF ENGINEERING AND SCIENCES

OF BILKENT UNIVERSITY

IN PARTIAL FULFILLMENT OF THE REQUIREMENTS

FOR THE DEGREE OF

MASTER OF SCIENCE

By

OĞUZHAN ÇELEBİ

May 2007

I certify that I have read this thesis and that in my opininon it is fully adequate, in scope and in quality, as a thesis of the degree of Master of Science

Prof. Dr. Hasan N. Erten (Advisor)

I certify that I have read this thesis and that in my opininon it is fully adequate, in scope and in quality, as a thesis of the degree of Master of Science

Prof. Dr. Ömer Dağ

I certify that I have read this thesis and that in my opininon it is fully adequate, in scope and in quality, as a thesis of the degree of Master of Science

Prof.Dr. Hale Göktürk

I certify that I have read this thesis and that in my opininon it is fully adequate, in scope and in quality, as a thesis of the degree of Master of Science

Assoc. Prof. Dr. Oğuz Gülseren

I certify that I have read this thesis and that in my opininon it is fully adequate, in scope and in quality, as a thesis of the degree of Master of Science

Assist. Prof. Dr. Emrah Özensoy

Approved for the Institute of Engineering and Sciences

Prof.Dr. Mehmet Baray

Director of Institute of Engineering and Science

ABSTRACT

INVESTIGATION OF THE ADSORPTION BEHAVIOR OF CESIUM, BARIUM AND PHENOL ONTO MODIFIED HUMIC ACID AND IRON NANOPARTICLES

OĞUZHAN ÇELEBİ
M.S. in Chemistry
Supervisor: Prof. Dr. Hasan N. Erten
May 2007

There is an increasing effort for removing highly soluble radiocontaminants from aqueous waste streams by fixing them onto solid waste forms that can be disposed of in a repository. In this way, the high-volume aqueous streams are transformed from a high-level radioactive waste into a low-level radioactive waste that is much cheaper to treat. However, the removal of this species may not only serve environmental initiatives, but it may also serve as a means of producing useful materials for use in science and industry. It is known, for example, that ^{137}Cs is an excellent γ source for medical applications such as instrument disinfection and radiotherapy. Similarly, ^{137}Cs has also proven to be useful as source for sterilization in the food industry. The radionuclide ^{137}Cs is produced in high yield during the fission process and due to its long half-life ($T_{1/2}$ = 30.17 y) and its high solubility in aqueous media, it is a principal radiocontaminant in radioactive wastes. Barium is an alkaline earth element (Z = 56), its radioactive isotope ^{140}Ba ($T_{1/2}$ = 12.79 d) is a fission product with a high yield (6.21%).

Wastewaters containing phenolic compounds present a serious environmental problem. Phenolic compounds are present in the wastewater generated from paint, solvent, petroleum (petrochemical), coal conversion etc. industries. Phenolic substances are known carcinogenic substances, doses over 1 g can be fatal for humans. Living organisms in aquatic environments are negatively effected by the uptake of phenolic subtances.

Humic acid , which is the most important organic component of soil, is a chemically and physically heterogeneous substance which is formed by chemical and biological degradation of organic residues in natural environment. Humic acid has many functions in soil chemistry such as adsorbing metal ions and organic substances, mineralization of plants and conversion of toxic substances biologically. Iron nanoparticle technology is increasingly being used in environmental remediation and hazardous waste treatment. One important advantage of nano-sized Fe^0 used in conventional permeable reactive barriers is that nanoparticles may be delivered to deep contamination zones by injection.

This study was conducted to find an alternative and efficient way for removing radioactive and phenolic wastes from aquatic environments. Modified humic acids (sodium form of insolubilized humic acid (INaA) and surfactant modified insolubilized humic acid (SMIA)) and iron nanoparticles were used as sorbent materials.

In this study, radioactive tracer method and UV-VIS spectroscopic technique were used to examine the sorption behavior of Cs^+, Ba^{2+} ions and phenol onto modified humic acids and iron nanoparticles. Characterization studies of humic acid and its modified forms were carried out using FTIR, solid state ^{13}C NMR spectroscopy techniques and adsorption sites (carboxylic and phenolic groups) of humic acid were quantitatively determined by potantiometric titration. SEM and PXRD techniques were used to characterize iron nanoparticle samples.

Sorption studies at different temperatures and kinetic studies were carried out to examine the effects of time, concentration, and temperature on the sorption of cations and phenol onto the various forms of humic acid and iron nanoparticles. All cation sorption processes are well described by both Freundlich and Dubinin-Radushkevich type isotherms. Phenol sorption data was well fitted to Freundlich and Tempkin isotherms when surfactant modified humic acid was used as a sorbent. The sorption order with cation sorbent pair is barium-INaA > cesium-INaA > barium- iron nanoparticles. Kinetic studies indicated that adsorption behaviors of both cations and phenol obey pseudo second order rate law. The rate constant values of the three sorption cases studied have an inverse relationship with sorption

affinity. The order for the rate of sorption with cation-sorbent pairs is as the following; barium-iron nanoparticles > cesium-INaA > barium-INaA. The equilibrium time for phenol sorption onto surfactant modified insolubilized humic acid was much longer than the equilibrium time for cations.

Thermodynamic parameters such as enthalpy change, ΔH^o , entropy change, ΔS^o and free energy of adsorption, ΔG^o, were calculated from the sorption data of Cs^+ and Ba^{2+} ions at different temperatures. The values obtained for ΔH^o and ΔS^o were -3.673 kJ/mol, 48.85 J/mol.K, 2.102 kJ/mol, 89.522 J/mol.K and -38.5 kJ/mol, -73.98 J/mol.K for cesium-INaA, barium-INaA and barium-iron nanoparticles ion-sorbent pairs, respectively. Temperature changes did not siginificanly affect the sorption affinity of Cs^+ and Ba^{2+} ions onto INaA. Ba^{2+} ion sorption onto iron nanoparticles is an exothermic process which means that low temperatures are favored.

The calculated negative values of ΔG^o obtained at different temperatures indicate the spontaneity of all adsorption processes studied. All adsorption mean free energy values are found to be within 8-16 kj/mol range which is the energy range of ion-exchange type processes.

Keywords: Adsorption, Isotherms, Modified Humic Acid, Thermodynamic Constants, Phenol, Kinetic Studies, Distribution Ratio, Radioactive Tracer Method, Cesium, Barium, Batch Method, Characterization, Iron Nanoparticles, UV-VIS spectroscopy.

ÖZET

SEZYUM, BARYUM VE FENOLÜN YAPISI DEĞİŞTİRİLMİŞ HÜMİK ASİT VE DEMİR NANOPARÇACIKLAR ÜZERİNE TUTUNMASININ İNCELENMESİ

OĞUZHAN ÇELEBİ
Kimya Bölümü Yüksek Lisans
Tez Yöneticisi : Prof. Dr. Hasan N. Erten
Mayıs 2007

Yüksek çözünürlüğe sahip olan radyoaktif maddelerin sıvı ortamlardan katı ortamlara aktarılarak depolarda tutulması yönünde çok miktarda çalışma yapılmaktadır. Bu sayede yüksek hacme sahip sıvı ortamlardaki radyoaktif maddelerin katı ortama aktarılması amaçlanmaktadır. Bu tür maddelerin çevresel uygulamalarda kullanılmasının yanı sıra bilim ve sanayide yararlı maddelerin üretilmesinde kullanılabilir. ^{137}Cs izotopunun dezenfeksiyon ve radyoterapi gibi medikal uygulamalarda γ kaynağı olarak kullanıldığı bilinmektedir. Benzer şekilde ^{137}Cs izotopu gıda endüstrisinde sterilizasyon kaynağı olarak yararlı bir madde olduğu kanıtlanmıştır. ^{137}Cs radyoizotopu radyoaktif bölünme sonucu yüksek verimde üretilir, uzun bir yarılanma süresi (30.17 yıl) ve yüksek çözünürlüğe sahip olduğu için radyoaktif atıklarda bulunan başlıca maddedir. Baryum bir toprak alkali elementi olup radyoaktif izotopu olan ^{140}Ba ($T_{1/2}$ = 12.79 gün) yüksek oranda (6.21%) açığa çıkan bir radyoaktif bölünme ürünüdür.

Fenolik maddeler içeren atık sular ciddi bir çevre problemi oluşturmaktadırlar. Fenolik maddeler boya, çözücü, petrokimya, kömür vb. sanayilerinden çevreye bırakılmaktadırlar ve kanserojen madde olarak bilinmektedirler. İnsanlar tarafından bir gramdan fazla alındığı durumlarda ölümcül etki yapmaktadırlar. Sıvı bölgelerde yaşayan organizmalar fenolik maddelere maruz kalmalarından ötürü olumsuz yönde etkilenmektedirler.

Toprağın en önemli organik maddesi olan hümik asit, doğal çevrede bulunan organik kalıntıların kimyasal ve fiziksel olarak parçalanmasıyla oluşturulan kimyasal ve fiziksel yönden heterojen bir maddedir. Hümik asitin toprak kimyasında metal iyonlarını ve organik maddeleri tutma, bitkilere mineral taşıma ve toksik maddeleri biyolojik olarak dönüştürmek gibi pek çok fonksiyonu vardır. Demir nanoparçacık teknolojisi artan bir hızla çevre ve zararlı atık uygulamalarında kullanılmaktadır. Önemli bir avantajı ise toprağın alt kısımlarında kalan kirli bölgeye enjeksiyon yöntemiyle rahatlıkla ulaştırılabilmesidir.

Bu çalışma radyoaktif ve fenolik atıkların sıvı ortam içeren çevrelerden uzaklaştırılması yönünde alternatif ve verimli bir yol bulmak için yapılmıştır. Yapısı değiştirilmiş hümik asitler (çözünmez hale getirilmiş hümik asitin sodyum formu ve yüzey aktif maddelerle değiştirilmiş hümik asit) ve demir nanoparçacıklar tutucu maddeler olarak kullanılmıştır. Radyoaktif izleme metodu ve UV-VIS spektroskopi tekniği kullanılarak sezyum, baryum iyonları ve fenolün değiştirilmiş hümik asitler ve demir nanoparçaklar üzerine tutunma davranışları incelenmiştir.

Hümik asit ve değiştirilmiş yapılarının karakterizasyonu FTIR, katı hal ^{13}C NMR spektroskopi teknikleri kullanılarak yapılmıştır. Hümik asit üzerinde tutunmadan sorumlu olan karboksilik ve fenolik gruplar potansiyometrik titrasyon metodu kullanarak miktarsal olarak tayin edilmiştir. Demir nanoparçacık örneklerini karakterize etmek için SEM ve PXRD teknikleri kullanılmıştır.

Zaman, konsantrasyon ve sıcaklığın, katyonların ve fenolün hümik asitin değiştirilmiş yapıları ve demir nanoparçacıklar üzerine tutunması üzerine etkisini incelemek için, farklı sıcaklıklarda tutunma çalışmaları ve kinetik çalışmalar yapıldı. Sezyum ve baryum tutunma verilerinin Freundlich ve Dubinin-Radushkevich modellerine, fenol tutunma verilerinin ise Freundlich ve Tempkin modellerine en iyi uyduğu bulunmuştur. Katyon ve tutucu madde tutunma sırası baryum-çözünmez hale getirilmiş hümik asit > sezyum-çözünmez hale getirilmiş hümik asit > baryum-demir nanoparçacıklar şeklindedir. Kinetik çalışmalar her iki katyonun ve fenolün tutunma davranışlarının psödo ikinci derece hız yasasına uyduğunu göstermiştir. Hız sabiti değerleri tutunma sırasıyla ters orantılıdır. Katyon tutucu maddelere tutunma hızı baryum-demir nanoparçacıklar > sezyum-çözünmez

hale getirilmiş hümik asit > baryum-çözünmez hale getirilmiş hümik asit sırasını takip etmektedir. Fenolün yüzey aktif maddelerle yapısı değiştirilmiş hümik asit üzerine tutunmasının dengeye ulaşma zamanının katyonların çözünmez hale getirilmiş hümik asit üzerine tutunmasının dengeye ulaşma zamanından çok daha fazla olduğu bulunmuştur.

Adsorpsiyon entalpi değişimi, ΔH^o, entropi değişimi, ΔS^o ve Gibbs serbest enerji değişimi, ΔG^o gibi termodinamik değerler farklı sıcaklıklarda elde edilen tutunma verilerinden elde edilen sonuçlar kullanılarak hesaplanmıştır. ΔH^o ve ΔS^o için elde edilen değerler sezyum iyonlarının çözünmez hale getirilmiş hümik asit üzerine tutunması için 3.673 kJ/mol, 48.85 J/mol.K, baryum iyonlarının çözünmez hale getirilmiş hümik asit üzerine tutunması için 2.102 kJ/mol, 89.522 J/mol.K ve baryum iyonlarının demir nanoparçacıklar üzerine tutunması için -38.5 kJ/mol, -73.98 J/mol.K olarak bulunmuştur. Sıcaklık değişimlerinin, sezyum ve baryum iyonlarının çözünmez hale getirilmiş hümik asit üzerine tutunma eğiliminde çok fazla etki yapmadığı bulunmuştur. Baryum iyonlarının demir nanoparçacıklar üzerine tutunma davranışları ekzotermiktir ve düşük sıcaklıklarda daha fazla katyon tutulduğunu göstermektedir.

Farklı sıcaklıklarda yapılan çalışmalar sonucu elde edilen sonuçları kullanarak yapılan hesaplamalarda bulunan negatif Gibbs serbest enerji değişimi, ΔG^o, değerleri bütün adsorpsiyon süreçlerinin kendiliğinden oluştuğunu göstermektedir. Hesaplanan ΔG^o değerlerinin tümü, 8-16 kJ/mol değerleri arasında bulunmaktadır. Bu düzeydeki enerjiler, adsorpsiyonun daha çok iyon değişimi yoluyla meydana geldiğini göstermektedir.

Anahtar kelimeler: Adsorpsiyon, İzotermler, Modifiye Edilmiş Hümik asit, Termodinamik Sabitler, Fenol, Kinetik Çalışmalar, Dağılım Oranı, Radyoaktif İzleme Metodu, Sezyum, Baryum, Tekne Tekniği, Karakterizasyon, Demir Nanoparçacıklar, UV-VIS Spektroskopi.

ACKNOWLEDGEMENT

I would like to express my sincere gratitude to my advisor, Prof. Dr. Hasan Erten, for his encouragement and tremendous support throughout my graduate career. I appreciate his patience and confidence in me from the first day. I would like to thank my current committee members, Prof. Dr. Ömer Dağ, Prof. Dr. Hale Göktürk, and Assoc. Prof. Dr. Oğuz Gülseren, Assist. Prof. Dr. Emrah Özensoy, for their valuable time and guidance during my graduate studies at Bilkent University.

I would also like to thank Prof. Dr. Şefik Süzer for his help and guidance during my graduate studies. I would particularly like to thank my undergraduate supervisor Prof.Dr. Yaşar Dürüst for his initiative support and mentorship when I first stepped into the research world. I would like to send my gratitude to my professors at Abant Izzet Baysal and Bilkent Universities who always encouraged and supported me throughout my undergraduate and graduate studies.

I would like to thank my dear colleagues : Muharrem Akcan, Cevher Altuğ, Yaşar Akdoğan, A. Faik Demirörs, Anıl Ağıral, Ünsal Koldemir, Hacı Osman Güvenç, Cemal Albayrak, Yurdanur Türker, Olga Samarskaya, İlknur Tunç, Li Yan, Nesibe Cındır, Burak Tiftik, Hikmet Sezen, Mehtap Küyükoğlu, Korcan Demirok, İlknur Çayırtepe, M.Fatih Genişel, Bora İnci, Eda Özkaraoğlu, Engin Karabudak, Ümit Akbey, Alper Duru and Mehmet Göllü.

I can`t just thank my parents, Selami and Emine Çelebi, and my sister, Dilruba Çelebi, who have always trusted in me and supported me from the first day. I would not have been where I am today without my family.

Finally, my thanks especially go to my best friends, Gürkan Çakır and Haydar Türköz, and roommates, Erkan Okuyan and S. Tuncer Erdoğan, who have made life easier and more fun.

TABLE OF CONTENTS

1. INTRODUCTION 1

1.1- Hazardous Wastes 1

1.1.1- Radioactive Wastes 2

1.1.2- Phenolic Wastes 4

1.2- The Adsorption Process in Soil Organic Matter 5

1.3- Cation Exchange Capacity in Soils 7

1.4- Radioactive Tracer Method 9

1.5- The Batch Method 9

1.6- Gamma Ray Spectroscopy 10

1.7- UV-Visible Spectroscopy 10

1.8- The Present Study 11

1.8.1- Humic Acid and Modified Forms 11

1.8.2- Iron Nanoparticles 14

1.8.3- Cations and Their Radioactive Isotopes 16

2. EXPERIMENTAL 17

2.1- Isolation, Insolubilization and Surfactant Modification of Humic Acid 17

2.2- Quantitative Determination of Adsorption Sites on Humic Acid 17

2.3- Adsorption Experiments 18

2.3.1- Radioactive Tracer Method 18

2.3.2- Kinetic Studies 18

2.3.3- Effect of Loading, Temperature and pH 19

2.4 Spectroscopic Characterization of Humic Acid, Its Modified Forms and Iron Nanoparticles and Analysis of Phenol Solutions 20

2.4.1 Fourier Transform Infrared Spectroscopy 20

2.4.2 13C CP/MAS Nuclear Magnetic Resonance Spectroscopy 20

2.4.3 Powder X-Ray Diffraction 20

2.4.4 UV-Visible Spectrophotometer 20

2.4.5 Scanning Electron Microscope 21

3. RESULTS AND DISCUSSIONS 22
3.1- Characterization of Sorbents 22
3.1.1- Potantiometric Titration 22
3.1.2- Characterization of Humic acid and Its Modified Forms 24
3.1.3- Characterization of Iron Nanoparticles 27
3.2- Radiochemical Sorption Studies 29
3.2.1- Kinetic Studies 29
3.2.2- Loading and Temperature Studies 37
3.2.2.1- Loading Curves 37
3.2.2.2- Effect of pH 42
3.2.2.3- Freundlich Isotherm 43
3.2.2.4- Dubinin-Radushkevich (D-R) Isotherms 48
3.2.2.5- Thermodynamic Results 53
3.2.3- Effect of surfactant modification upon phenol and cation sorption affinity 59
3.2.3.1- Sorption studies using UV-VIS spectroscopy 59
3.2.3.1.1- Kinetic Studies 59
3.2.3.1.2- Freundlich and Tempkin isotherms for phenol sorption 63
3.2.3.2- Sorption studies of cesium onto surfactant modified insolubilized humic acid 67

4. CONCLUSION 70

REFERENCES 72

LIST OF FIGURES

1.1 Scheme of interactions of hazardous wastes in the environment 1
1.2 Scheme of interactions of hazardous wastes in the anthrosphere 2
1.3 Scheme of interactions between nucleus and neutron 3
1.4 Scheme of development of variable negative charges in a humic molecule by dissociation of protons from carboxyl groups at pH 3.0, and from phenolic-OH groups at pH 9.0. 6
1.5 Scheme of interactions between humic acid and a metal cation.. 6
1.6 Proposed structures of humic acid 12
1.7 Scheme of hydrophobic interactions in surfactant-humic acid system 14
1.8 TEM images of iron nanoparticles 16
3.1 Potantiometric titration curve of humic acid 23
3.2 Linearized plot potantiometric titration curve of humic acid using Gran function 23
3.3 FTIR spectra of humic acid and sodium form of insolubilized humic acid . 25
3.4 13C NMR spectra of humic acid and sodium form of insolubilized humic acid 26
3.5 FTIR spectra of sodium form of insolubilized humic acid and surfactant modified insolubilized humic acid 26
3.6 XRD Pattern for nano-Fe0 and its oxide form 27
3.7 SEM images of iron nanoparticles at different magnifications 28
3.8 Variation of Rd Values with Shaking time for Cs+ sorption onto sodium form of insolubilized humic acid at 25°C 30
3.9 Variation of Rd Values with Shaking time for Ba2+ sorption onto sodium form of insolubilized humic acid at 25°C 31
3.10 Variation of Rd Values with Shaking time for Ba2+ sorption on iron nanoparticles at 25°C 31
3.11 Variation of t/q Values with Shaking time for Cs+ sorption on sodium form of insolubilized humic acid at 25°C 35

3.12 Variation of t/q Values with Shaking time for Ba2+ sorption on sodium form of insolubilized humic acid at 25°C 35
3.13 Variation of t/q Values with Shaking time for Ba2+ sorption on iron nanoparticles at 25°C 36
3.14 The loading curves for sorption of Cs+ onto sodium form of insolubilized humic acid at different temperatures 38
3.15 The loading curves for sorption of Ba2+ onto sodium form of insolubilized humic acid at different temperatures 38
3.16 The loading curve for sorption of Ba2+ onto iron nanoparticles at 25°C .. 39
3.17 The loading curve for sorption of Ba2+ onto iron nanoparticles at 55°C .. 39
3.18 Effect of pH upon sorption of Ba2+ onto sodium form of insolubilized humic acid 42
3.19 Freundlich isotherm plots for the sorption of Cs+ onto sodium form of insolubilized humic acid at various temperatures 45
3.20 Freundlich isotherm plots for the sorption of Ba2+ onto sodium form of insolubilized humic acid at various temperatures 45
3.21 Freundlich isotherm plots for sorption of Ba2+ onto iron nanoparticles at 25˚C and 55˚C 46
3.22 Freundlich isotherm plots for sorption of Ba2+ onto iron nanoparticles at 25˚C with different weights 25mg, 50mg and 100mg 46
3.23 Dubinin-Radushkevich isotherm plots for sorption of Cs+ onto sodium form of insolubilized humic acid at various temperatures 50
3.24 Dubinin-Radushkevich isotherm plots for sorption of Ba2+ onto sodium form of insolubilized humic acid at various temperatures 50
3.25 Dubinin-Radushkevich isotherm plots for sorption of Ba2+ onto iron nanoparticles at 25˚C and 55˚C 51
3.26 Dubinin-Raduskevich isotherm plots for sorption of Ba2+ onto iron nanoparticles at 25˚C with different weights 25mg, 50mg and 100mg 51
3.27 Arrhenius plots for sorption of Cs+ onto sodium form of insolubilized humic acid 56
3.28 Arrhenius plots for sorption of Ba2+ onto sodium form of insolubilized humic acid 56
3.29 Arrhenius plots for Sorption of Ba2+ onto iron nanoparticles 57

3.30 UV-Vis absorption spectra of phenol solutions remaining in solution after sorption at different shaking times 60
3.31 Variation of Rd values with shaking time for phenol sorption onto surfactant modified insolubilized humic acid at 25°C 61
3.32 Variation of t/q Values with Shaking time for Ba2+ sorption onto surfactant modified insolubilized humic acid at 25°C 61
3.33 Freundlich Isotherm plot for sorption of phenol onto surfactant modified insolubilized humic acid at 25˚C 64
3.34 Tempkin isotherm plot for sorption of phenol onto surfactant modified insolubilized humic acid at 25˚C 65
3.35 The loading curve for sorption of Cs^{+} onto surfactant modified insolubilized humic acid at 25ºC 67
3.36 Dubinin-Radushkevich isotherm plot for sorption of Cs+ onto surfactant modified insolubilized humic acid at 25˚C 68
3.37 Freundlich isotherm plots for sorption of Cs+ onto surfactant modified insolubilized humic acid at 25˚C 69

LIST OF TABLES

1.1 Cation Exchange Capacities for a Number of Soil Colloids 8
3.1 Acidic functional group contents obtained experimentally using potantiometric titration of humic acid 24
3.2 The sorption data for the kinetic behavior Cs+ ion on sodium form of insolubilized humic acid..... 32
3.3 The sorption data for the kinetic behavior Ba2+ ion on sodium form of insolubilized humic acid..... 32
3.4 The sorption data for the kinetic behavior Ba2+ ion on iron nanoparticles..... 33
3.5 Amount of sorbed cation per gram of sorbent, pseudo second order rate constants and correlation coefficient values for cesium and barium sorption . 36
3.6 The data of Cs+ sorption onto sodium form of insolubilized humic acid at different temperatures and initial concentrations 40
3.7 The data of Ba2+ sorption onto sodium form of insolubilized humic acid at different temperatures and initial concentrations 40
3.8 The data of Ba2+ sorption onto iron nanoparticles at different temperatures and initial concentrations 41
3.9 Freundlich constants , n and k , obtained from the least square fits of the sorption data of Cs+ onto sodium form of insolubilized humic acid..... 47
3.10 Freundlich constants , n and k , obtained from the least square fits of the sorption data of Ba2+ onto sodium form of insolubilized humic acid..... 47
3.11 Freundlich constants, n and k, obtained from the least square fits of the sorption data of Ba2+ onto iron nanoparticles 47
3.12 The D-R Isotherm constants obtained from the least square fits for the sorption data of Cs+ onto sodium form of insolubilized humic acid..... 52
3.13 The D-R Isotherm constants obtained from the least square fits for the sorption data of Ba2+ onto sodium form of insolubilized humic acid..... 52
3.14 The D-R Isotherm constants obtained from the least square fits for the sorption data of Ba2+ onto iron nanoparticles 52

3.15 The average values of the enthalpy change, entropy change and the calculated values of the Gibbs Free Energy change obtained at different temperatures for the sorption case of Cs+ onto sodium form of insolubilized humic acid 57
3.16 The average values of the enthalpy change, entropy change and the calculated values of the Gibbs Free Energy change obtained at different temperatures for the sorption case of Ba2+ onto sodium form of insolubilized humic acid..... 58
3.17 The average values of the enthalpy change, entropy change and the calculated values of the Gibbs Free Energy change obtained at different temperatures for the sorption case of Ba2+ onto iron nanoparticles 58
3.18 The kinetic data of phenol sorption onto surfactant modified insolubilized humic acid at different times at 25ºC 62
3.19 Amount of sorbed phenol per gram of sorbent, pseudo second order rate constant and correlation coefficient value for phenol sorption 62
3.20 Freundlich constants , n and k , obtained from the least square fits of the sorption data of phenol onto surfactant modified insolubilized humic acid .. 64
3.21 Tempkin isotherm constants obtained from the least square fits of the sorption data of phenol onto surfactant modified insolubilized humic acid. 65
3.22 The data of phenol sorption onto surfactant modified insolubilized humic acid at 25ºC and initial concentrations..... 66
3.23 The D-R Isotherm constants obtained from the least square fits for the sorption data of Cs+ onto surfactant modified insolubilized humic acid..... 68
3.24 Freundlich constants , n and k , obtained from the least square fits of the sorption data of Cs+ onto surfactant modified insolubilized humic acid 69

1. INTRODUCTION

1.1- Hazardous Wastes

A hazardous substance is a material that may pose a danger to living organisms, materials, structures or environment. Hazardous waste is a hazardous substance that has been discarded, abandoned, neglected, released or designated as a waste material, or one that might interact with other substances to be hazardous.

Many specific chemicals in widespread use are hazardous because of their chemical reactivities, fire hazards, toxicities, and other properties. There are numerous kinds of hazardous substances, usually consisting of mixtures of specific chemicals. These include such things as explosives; flammable liquids and solids, oxidizing materials, corrosive materials, and radioactive materials.

Hazardous materials almost always originate in the anthrosphere – which is part of the environment that is made or modified by humans for use in human activities- are often discarded into the geosphere, and are frequently transported through the hydrosphere or the atmosphere. The greatest concern for their effects is usually on the biosphere, particularly human beings. Figures (1.1 and 1.2) summarize these relationships.[1]

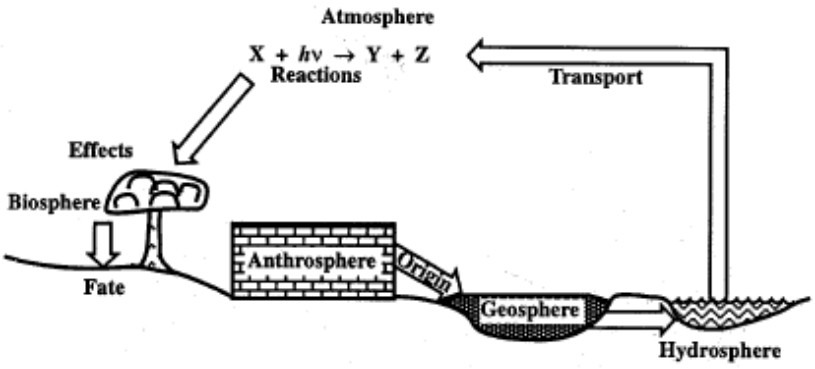

Fig. 1.1: Scheme of interactions of hazardous wastes in the environment[1]

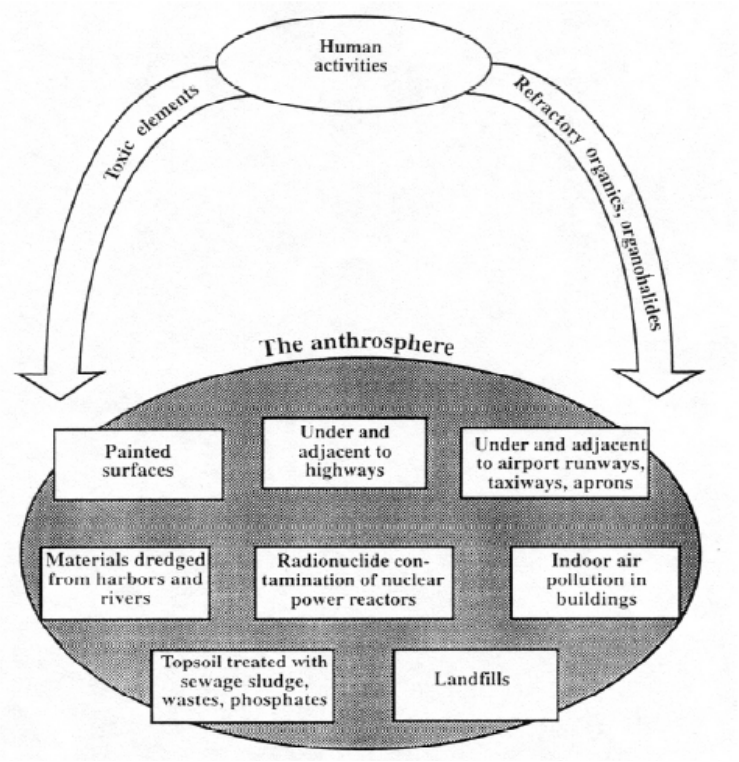

Fig. 1.2: Scheme of interactions of hazardous wastes in the anthrosphere[1]

1.1.1- Radioactive Wastes

The massive production of radionuclides (radioactive isotopes) by weapons and nuclear reactors since World War II has been accompanied by increasing concern about the effects of radioactivity upon health and the environment. Radionuclides are produced as fission products of heavy nuclei of such elements as uranium or plutonium. They are also produced by the reaction of neutrons with stable nuclei. These phenomena are illustrated in Fig. 1.3. Radionuclides are formed in large quantities as waste products in nuclear power generation. Their ultimate disposal is a problem that has caused much controversy regarding the widespread use of nuclear power. Artificially produced radionuclides are also widely used in industrial and medical applications, particularly as "tracers." With so many possible sources of radionuclides, it is impossible to entirely eliminate radioactive contamination of aquatic systems. Furthermore, radionuclides may enter aquatic systems from natural sources. Therefore, the transport, reactions, and biological concentration of radionuclides in aquatic ecosystems are of great importance to the environmental chemist.

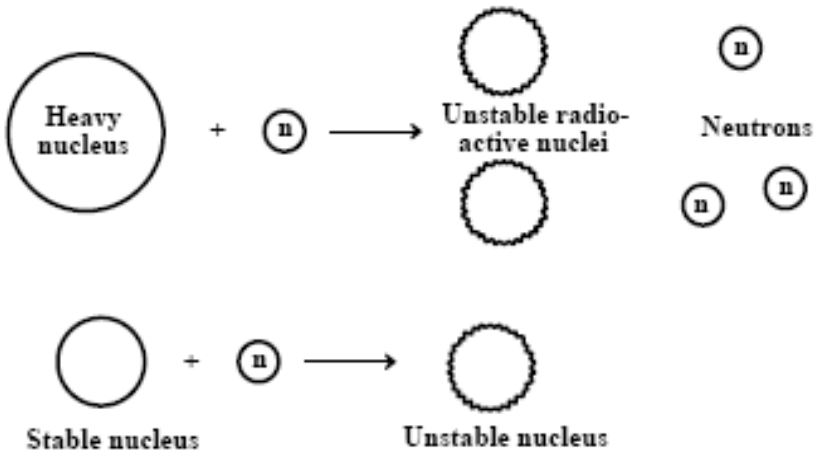

Fig. 1.3: Scheme of interactions between nucleus and neutron

Radiation damages living organisms by initiating harmful chemical reactions in tissues. For example, bonds are broken in the macromolecules that carry out life processes. In cases of acute radiation poisoning, bone marrow that produces red blood cells is destroyed and the concentration of red blood cells is diminished. Radiation-induced genetic damage is of great concern. Such damage may not become apparent until many years after exposure. As humans have learned more about the effects of ionizing radiation, the dosage level considered to be safe has steadily diminished.

The study of the ecological and health effects of radionuclides involves consideration of many factors. Among these are the type and energy of radiation emitted and the half-life of the source. In addition, the degree to which the particular element is absorbed by living species and the chemical interactions and transport of the element in aquatic ecosystems are important factors. Radionuclides with intermediate half-lives are the most dangerous. They persist long enough to enter living systems while still retaining a high activity. Because they may be incorporated within living tissue, radionuclides of life elements are particularly dangerous.[1]

Many alternatives for radioactive waste treatment have been investigated and some of them have been applied successfully in the waste treatment plants.

However, no method is universally applicable and the adoption of any treatment technique for a given type of waste will depend on efficiency of the method, characteristics of the waste, availability of the material and economical consideration.[2]

There is an increasing effort for removing highly soluble radiocontaminants from high volume aqueous waste streams by fixing them onto solid waste forms that can be disposed of in a repository. In this way, the high-volume aqueous streams are transformed from a high-level radioactive waste into a low-level radioactive waste that is much cheaper to treat. However, the removal of this species may not only serve environmental initiatives, but it may also serve as a means of producing useful materials for use in science and industry. It is known, for example, that ^{137}Cs is an excellent γ source for medical applications such as instrument disinfection and radiotherapy. Similarly, ^{137}Cs has also proven to be useful as source for sterilization in the food industry.[3] The overall objective of radioactive waste disposal is to dispose the wastes in a manner which ensures that there is no unacceptable detriment to man and to the biological environment, as a whole at present and in the future. Waste confinement by the disposal system should remain effective until the radionuclides have decayed to acceptable levels, and are no longer forming a potential hazard to the human environment.[4]

1.1.2- Phenolic Wastes

Wastewaters containing phenolic compounds present a serious environmental problem. Phenolic compounds are present in the wastewater generated from paint, solvent, petroleum (petrochemical), coal conversion, pharmaceutical, wood preserving chemicals- plastic, rubber-proofing, pesticide, iron-steel, phenol-production, paper and pulp industries. Phenolic substances are known carcinogenic substances and concentrations greater than 50 ppb are harmful to some aquatic species and ingestion of 1 g can be fatal in humans therefore phenol removal from waters is an important practical problem.

Current methods for removing phenols and their derivatives from wastewater include microbial degradation, adsorption on sorbents, biosorption, chemical oxidation, deep-well injection, incineration, solvent extraction and irradiation.[5,6]

1.2- The Adsorption Process in Soil Organic Matter

Adsorption is a general term that refers to the disappearance of solutes from solution with the presumption of adsorption on a solid phase. Adsorption is the accumulation at the solid-solution interface, and may result from either physical, electrostatic or chemical interactions with the surface. Physical and electrostatic types of adsorptions form relatively weak bonds to the surface whose characteristic energies are 4.2-8.4 kJ/mol and 8-16 kJ/mol, respectively, while chemical adsorption is a stronger interaction which involves ionic or covalent bonding whose characteristic energy is 100-500 kj/mol. Adsorption refers to attraction and bonding onto a surface, while absorption is a process in which the solute is taken up into a structure. In some cases the distinction is difficult and the generic term sorption has been used. Operationally, sorption is determined by the extent of solute removal from solution in either batch studies or in leaching studies with columns of adsorptive materials.[7]

Adsorption is dependent not only on the surface charge, but also on the surface area. The amount of material adsorbed is directly proportional to the specific surface. Adsorption is small if the surface area is small, and increases with increased surface areas. Small surface area, together with its low cation exchange capacity, are the reasons for a low adsorption capacity.

Soils have the capacity to adsorb gas, liquid and solid constituents. Cation exchange reactions, complex reactions between metal ions, and inorganic and organic colloids are additional implications of the electrochemical behavior of soil colloids. The physico-chemical properties of soils are attributed to soil constituents with highly reactive surfaces and large surface areas, e.g., soil organic and

inorganic colloids. Therefore, this colloidal fraction plays a dominant role in adsorption phenomena.

Adsorption reactions take place at the surfaces of soil colloids. In the case of the organic colloids, e.g., humic matter, adsorption is related to reactions with their functional groups, such as carboxyl groups, and phenolic hydroxyl groups. The carboxyl group starts to dissociate its proton around pH 3.0, and the humic molecule becomes electronegatively charged (Fig. 1.4). At pH < 3.0, the charge is very small, or even zero. At pH 9.0, the phenolic-OH group also starts to dissociate, and the molecule attains a high negative charge. Since the development of negative charges is pH dependent, this charge is called pH-dependent charge. A number of reactions or interactions can take place because of the presence of these charges. At low pH values, the humic molecule is capable of attracting cations, which leads to cation exchange reactions. At high pH values, when the phenolic -OH groups are also dissociated, complex reactions and chelation between metals and the humic molecule are of importance (Fig. 1.5).

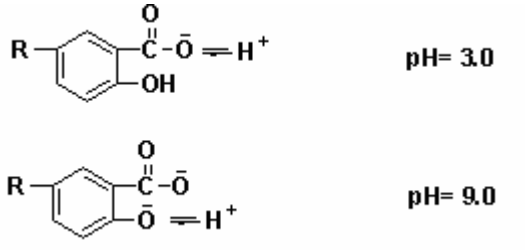

Fig. 1.4: Development of variable negative charges in a humic molecule by dissociation of protons from carboxyl groups at pH 3.0, and from phenolic-OH groups at pH 9.0.[8]

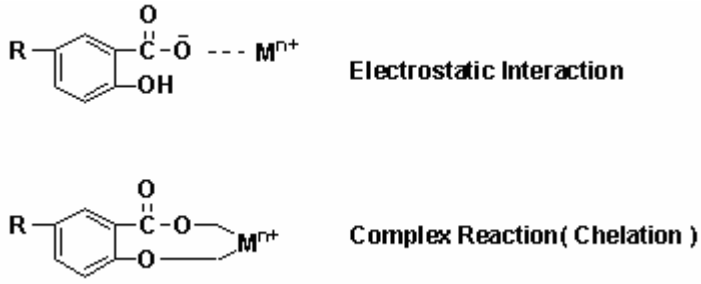

Fig. 1.5 Scheme of interactions between humic acid and a metal cation. M^{n+} = cation with charge n^+; R = remainder of humic acid molecule.[8]

The density of ion population is greatest at or near the surface. These cations are called adsorbed cations. Different rates and orders of adsorption are known among the cations, since the adsorption reaction depends on the surface potential, valence, and hydrated radius. As surface potential increases, more of the divalent ions will be adsorbed. Trivalent cations would even be more strongly concentrated on the surface exhibiting high surface potential values. When a mixture of monovalent and divalent ions are present in a soil solution, adsorption is usually shifted in favor of the divalent ions. Specific adsorption of cations is also affected by the hydrated radius. The crystalline radius, on the other hand, plays only a minor role. Generally, ions with smaller hydrated sizes are preferably adsorbed as compared to ions with larger hydrated sizes. The following is the decreasing order of preference for adsorption of monovalent cations by clays:

$$Cs^+ > Rb^+ > K^+ > Na^+ > Li^+$$

The rate of adsorption for Cs is the highest, because Cs is the smallest in hydrated size. The ion has a thin hydration shell, which makes a close approach to the surface possible. Lithium, on the other hand, has the largest hydrated radius in this series. Its thick hydration shell increases the distance from the ion to the clay surface.[8]

1.3- Cation Exchange Capacity in Soils

The process in which cations from solutions are sorbed by mineral particles with the concurrent release of an equivalent amount of cations is termed as cation exchange process. Cation exchange capacity (CEC) of a soil is defined as the capacity of soils to adsorp and exchange cations. Scientifically, it is related to the surface area and surface charge. CEC is commonly determined by extraction of the cations from soils with a solution containing a known cation for exchange. The results, expressed in milliequivalents per 100 grams of soils are taken as the CEC of soils. The values for CEC may vary considerably, depending on the concept used of

CEC, methods of analysis, type of colloids, and amount of colloids. On the average the CEC of the major soil colloids is as follows:

The affinity of a certain cation, M^+, for an exchange site is affected by several factors such as:

1- Concentration in solution: As $[M^{n+}]$ increases, there is an increase in the fractional surface coverage.

2- Oxidation state: An increase in the oxidation state of an element favors its accumulation at the surface, the order of affinity being:

$$M^{3+} > M^{2+} > M^{+}$$

3- Charge density of the hydrated cation: the greater the charge density, the greater is the affinity for an exchange site.

Table 1.1 Cation Exchange Capacities for a Number of Soil Colloids

Soil Colloids	**CEC (mEq/100g)**
Humus (Humic matter)	200
Vermiculite	100-150
Smectite	70-95
Illite	10-40
Kaolinite	3-15

Adsorption and cation exchange are of great practical significance in nutrient uptake by plants, soil fertility, nutrient retention, and fertilizer application. Its importance has increased considerably today by an increased awareness of its beneficial effect in environmental issues. It is realized now that cation exchange has the capacity in intercepting toxic metals and organic compounds reaching the groundwater and preventing pollution of streams and lakes.[4, 8]

1.4- Radioactive Tracer Method

The radioactive tracer method is one of the most useful techniques in radiochemistry which finds applications in many of the branches of sciences such as biological, medical, geological and environmental studies. The fundamental principle of the radioactive tracers is that the chemical behavior of radioactive isotopes is identical with that of their stable isotopes in any chemical process. The effect of radiation emitted by the radioactive tracers on a chemical or biological system under study is also usually negligible. The amount of a radioactive tracer necessary for an experiment is normally so small that no detectable radiolysis occurs in the system.[9]

The tracer method consists of the introduction of a small amount of a radionuclide and the observation of its progress as time goes on during sorption study. The decrease in the radionuclide concentration in solution is attributed to its sorption by the sorbent.

1.5- The Batch Method

The batch method is one of the most used technique in sorption studies. In a batch operation, the adsorbent is contacted with the liquid phase in a container for a period of time. The adsorbent is separated from the liquid by centrifugation, filtration or settling. The time required to approach equilibrium condition depends on the concentration of solute, amount of solid, the particle size of adsorbent and the degree of shaking.

For batch operations, adsorbent is usually applied in powdered form to increase the surface area and reduce the diffusional resistance inside the pores. Agitation of the suspension improves contact of particles with liquid and decreases the mass transfer resistance at the surface[4].

1.6- Gamma Ray Spectroscopy

Gamma spectroscopy is a radiochemical measurement method and a gamma spectrometer determine the energy and the count rate of gamma rays emitted by radioactive substances. In investigating a radioactive source, one generally finds gamma lines of various energies and intensities; the result is called a gamma energy spectrum. A detailed analysis of this spectrum is used to determine the identity and quantity of gamma emitters present in the source. The gamma spectrum is characteristic of the gamma emitting nuclides contained in the source, just as in optical spectroscopy, the optical spectrum is the characteristic of the atoms and molecules contained in the probe.

The equipment used in gamma spectroscopy includes an energy sensitive particle detector, a pulse sorter (multichannel analyzer), and associated amplifiers and data readout devices. The detector is often a sodium iodide (NaI) scintillation counter or a high purity germanium detector.[10]

1.7- UV-Visible Spectroscopy

Ultraviolet-visible spectroscopy uses light in the visible, adjacent near ultraviolet (UV) and near infrared ranges. In this region of energy space molecules undergo electronic transitions. UV-Visible spectroscopy is routinely used in the quantitative determination of solutions of transition metal ions and highly conjugated organic compounds.

The Beer-Lambert law states that the absorbance of a solution is due to the solution's concentration. Thus UV-Visible spectroscopy can be used to determine the concentration of a solution. It is necessary to know how quickly the absorbance changes with concentration. This can be taken from references (tables of molar extinction coefficients), or more accurately, determined from a calibration curve.

The method is most often used in a quantitative way to determine concentrations of an absorbing species in solution, using the Beer-Lambert law:

$$A = -\log_{10}(I/I_0) = \varepsilon.b.c$$

where A is the measured absorbance, I_0 is the intensity of the incident light at a given wavelength, I is the transmitted intensity, b the pathlength through the sample, and c the concentration of the absorbing species. For each species and wavelength, ε is a constant known as the molar absorptivity or extinction coefficient. This constant is a fundamental molecular property in a given solvent, at a particular temperature and pressure.[11]

1.8- The Present Study

In the present study, the adsorption behaviors of two important fission product radionuclides (^{137}Cs and ^{133}Ba) onto sodium form of insolubilized humic acid and iron nanoparticles were investigated as a function of time, cation concentration and temperature utilizing radioactive tracer method and a similar study was carried out for the adsorption behavior of phenol onto surfactant modified humic acid.

1.8.1- Humic Acid and Modified Forms

Humic substances are the most abundant reservoir of carbon on earth and perform various roles in soil chemistry. They act as soil stabilizers, nutrient and water reservoirs for plants, sorbents for toxic metal ions, radionuclides and organic pollutants, stimulate plant growth and biotransform toxic pollutants. When leached into surface waters, they also play a pivotal role in the aquatic environment. For example, they bind and transport metal ions.[12]

Early efforts to characterize this material resulted in the following fractionation scheme based on solubility under acidic or alkaline conditions: humin, the insoluble fraction of humic substances; humic acid, the fraction soluble under alkaline conditions but not acidic conditions (generally pH< 3); and fulvic acid, the fraction soluble under all pH conditions. Although chemical and physical differences do underlie these variations in solubility, the separation of humic

substances into three fractions is operational, and does not indicate, for example, the existence of three distinct types of organic molecule.

Early concepts, based on the developing field of polymer science assumed that humic substances comprised of randomly coiled macromolecules as shown in Fig. 1.6 that had elongated shapes in basic or low-ionic strength solutions, but became coils in acidic or high-ionic strength solutions.

However, recent information gathered using spectroscopic, microscopic, pyrolysis, and soft ionization techniques is not consistent with the "polymer model" of humic substances. A new concept of humic substances has thus emerged, that of the supramolecular association, in which many relatively small and chemically diverse organic molecules form clusters linked by hydrogen bonds and hydrophobic interactions (Fig. 1.6). A corollary to this model is the concept of micellar structure, i.e., an arrangement of organic molecules in aqueous solution to form hydrophilic exterior regions shielding hydrophobic interiors from contact with vicinal water molecules.[13]

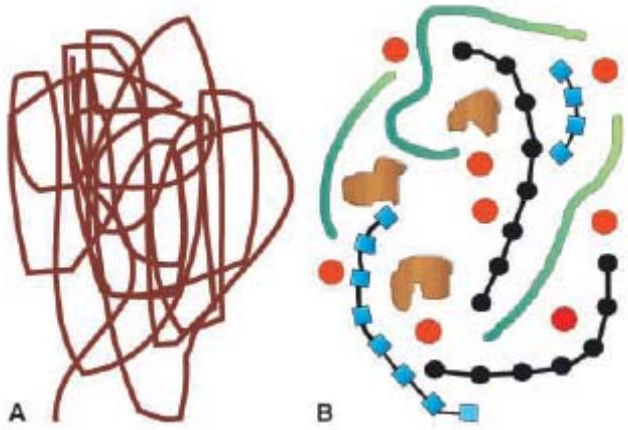

Fig. 1.6: **A** Depiction of the traditional concept of humic substances as randomly coiled macromolecules. **B** A new concept that the major components found in soil humic substances are in fact of relatively low molecular weight (<2,000 Da) and associate in the presence of metals to form an aggregate. The *red spheres* represent generic metal cations, the *black units* polysaccharides, the *blue units* polypeptides, the *green units* aliphatic chains, and the *brown units* aromatic lignin fragments.[14]

It is important to note that humic materials are complex mixtures of many components, which vary in ratio and structure with sample origin and extraction procedure. Therefore this concept should only be considered as an example of a humic aggregate that is not definitive. While aggregates will likely be "held together" through a complex combination of hydrophobic associations, charge interactions, hydrogen bonds, and metal bridging.

Humic acid is known as the insoluble fraction below pH<3 in aqueous media. This makes humic acid an inappropriate sorbent for traditional operations such as adsorption and recovery of metal ions in aqueous media. The solubility of humic acid in aqueous media depends on the number of –COOH and –OH groups present on humic acid on a large scale and with increasing content of these groups solubility increases. These groups also give humic acid the ability to interact with metal ions through adsorption, ion-exchange, and complexation mechanisms. However, the high solubility of humic acid in aqueous media is a limiting problem for taking advantage of the interaction ability of humic acid (as a solid phase) with metal ions. Accordingly, it is not advisable to use untreated humic acid as a sorbent in aqueous media, so an appropriate treatment of humic acid is needed.[15]

The process developed by Seki and Suzuki[16] is called "insolubilization of humic acid" and with this method humic acid can be converted to a form which is insoluble up to pH 10 in aqueous media.

Insolubilized humic acid has a negatively charged surface, therefore it is not a good sorbent for polar organic contaminants. Therefore a treatment is required to adsorb these type of compounds onto humic acid. It has been well recognized that ionic surfactants are cooperatively bound to polyelectrolytes with opposite charges. Insolubilized humic acid as a polyelectrolyte make strong interactions with cationic surfactants.

The electrostatic interaction between cationic head group of surfactant and anionic sites of humic acid is not the only driving force in the binding of surfactant. It is proposed that there are additional hydrophobic interaction between hydrophobic tail of surfactant and the hydrophobic part of humic acid.[17]

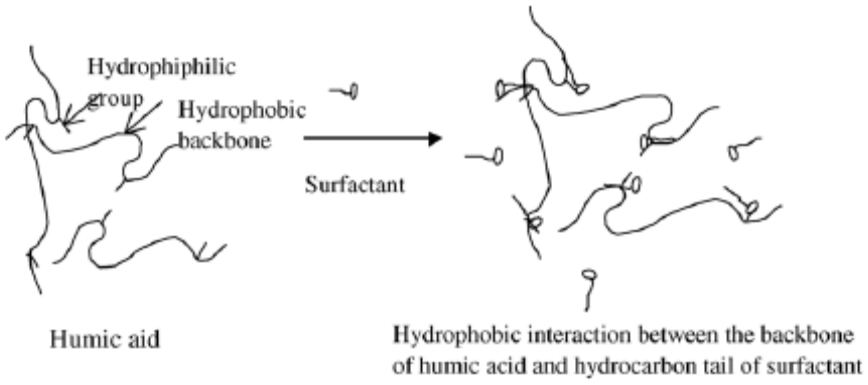

Fig. 1.7: Schematic representation of hydrophobic interactions in surfactant- humic acid system[17]

1.8.2- Iron Nanoparticles

Iron nanoparticle technology is increasingly being used in the environmental remediation and hazardous waste treatment. Nanoscale iron particles are effective for the transformation of a wide array of environmental contaminants such as chlorinated organic contaminants, organic dyes, and various inorganic compounds. Moreover, two potential advantages of nano-sized Fe° used in conventional permeable reactive barriers (PRBs) are that nanoparticles may be delivered to deep contamination zones by injection and that nano-sized Fe° may be more effective at degrading some contaminants than granular iron.

Reactivity of nano-Fe° suspensions can persist for at least 6-8 weeks. One reason that nano-sized Fe° particles might exhibit great rates of reaction with contaminants is simply that their large specific surface areas provide more sites on which reaction occurs. Other possible reasons why nano-Fe° might exhibit enhanced reactivity include higher density of reactive surface sites and greater intrinsic reactivity of surface sites.

Zerovalent iron (ZVI), due to its relatively low standard potential, is an inexpensive, efficient, and environmentally friendly electron donor:

$$Fe \rightarrow Fe^{2+} + 2e^{-} \qquad E^{0}_{ox} = -0.41\ V$$

$$Fe^{2+} \rightarrow Fe^{3+} + e^{-} \qquad E^{0}_{ox} = -0.771\ V$$

Ferrous iron, Fe^{2+}, can further donate an additional electron and be oxidized to ferric iron, Fe^{3+}. Many environmental contaminants serve as the ultimate electron acceptors. The dechlorination of chlorinated organic solvents such as tetrachloro-ethenes serve as a good example:

$$RCl + H^{+} + 2e^{-} \rightarrow RH + Cl^{-}$$

It is also known that, in water, iron reacts with water and forms a layer of oxyhydroxide:

$$Fe_{(s)} + 2H_2O_{(aq)} \rightarrow FeOOH_{(s)} + 1.5H_{2(g)}$$

Nanoparticles containing Fe° must be surrounded by some type of passivating layers such as a shell of oxides under environmental conditions (Fig. 1.8). Little work has been done to examine the sorption properties of zero valent iron. Specifically, the potential synergy of sorption and reduction has not been explored at all. The dual properties of sorption and reduction may yield new and unique applications of iron nanoparticles for contaminant separation and transformation.[18,19]

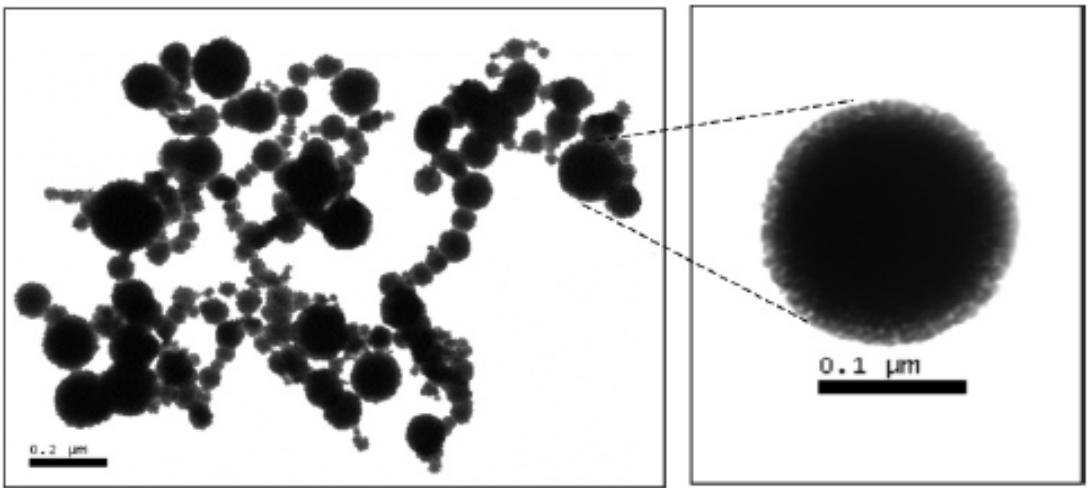

Fig 1.8: TEM images of iron nanoparticles[19]

1.8.3- Cations and Their Radioactive Isotopes

Barium is an alkaline earth element, radioactive isotope ^{140}Ba ($T_{1/2}$ = 12.79d) is a fission product with a high yield (6.21%). This radionuclide is a serious radiocontaminant, furthermore being a homologue of Ra, Ba^{2+} is a suitable cation for the radiochemical study of Ra^{2+}, which have several radioisotopes that are important in radioactive waste considerations. $^{133}Ba^{2+}$ was chosen as a radiotracer in our studies because of its long half-life ($T_{1/2}$ = 10.7 y) and a γ-ray at 356 keV energy.[20]

The radionuclide ^{137}Cs is produced in high yield (3-7% fission yield) during the fission process and due to its long half-life ($T_{1/2}$ = 30.17 y) and its high solubility in the aqueous media, it is a principal radiocontaminant in radioactive wastes.[21] It is widely used in tracer studies and a well-known gamma ray source.

2. EXPERIMENTAL

2.1- Isolation, Insolubilization and Surfactant Modification of Humic Acid

Humic acid was isolated from soil sample taken from Niğde (Bor) region by the following procedure; The soil sample was stirred in 1% NaOH solution for 1h and subsequently centrifuged at 5000 rpm. The dissolved fraction was taken and adjusted to pH 2 with HCl, stirred for 4h and subsequently centrifuged at 5000 rpm. The resulting precipitate was taken and this procedure was repeated two more times. The precipitate was rinsed with deionized water many times to remove chloride ions. After dechlorination step, humic acid was dried at 95 °C for 4h.

Humic acid was insolubilized by heating in a temperature controlled oven at 330°C for 1.5h and insolubilized humic acid (IHA) was converted to its sodium form (INaA) by stirring IHA in a 1M $NaNO_3$ solution for 2 days to exchange the acidic hydrogens with sodium ions, the resulting solid phase was dried at 80°C.

One hundred milliliters of concentrated cetyltrimethylammonium chloride solution was placed in a flask and 5 g of sodium form of insolubilized humic acid (INaA) added. The dispersions were shaken at room temperature by a mechanic shaker for 60 h, followed by washing with distilled water. The surfactant modified insolubilized humic acid (SMIA) was dried at 50 ˚C in an oven.

2.2- Quantitative Determination of Adsorption Sites on Humic Acid

Adsorption sites (carboxylic and phenolic groups) were determined quantitatively by using potantiometric titration method. Titration was carried out from pH 3.5 to 10.58 using 0.1M NaOH solution as titrant. Analyte was containing 50 ml suspension of humic acid (576 mg/l). This value was also used by other studies[42]. Nitrogen gas was passed through the solution until the end of titration in order to prevent CO_2 interference. The resulting data was linearized by using the appropriate Gran functions[22]. The total acidity value was taken to be the sum of carboxylic and phenolic acidities.

2.3- Adsorption Experiments

2.3.1- Radioactive Tracer Method

The batch method was applied throughout the study. The tracers used in sorption experiments were ^{137}Cs ($T_{1/2}$ = 30.17 y) and ^{133}Ba ($T_{1/2}$ = 10.7 y). 1 L of stable isotope solutions were spiked with ~ 400μL of the corresponding radionuclide solutions. The initial count rates were measured for 2.5 ml aliquots of cesium and barium solutions using the prominent γ rays of 662 and 361 keV, respectively. Initial acitivity was adjusted not to be lower than 10000 (cps)/ml.

A NaI(Tl) detector was used during radioactivity measurements of the samples. All the experiments were performed in duplicates. In order to check any loss in the activity originating from adsorption on the inside wall of tubes, blank experiments were performed using solutions without adsorbent. The results showed that adsorption onto the tube walls was negligible.

2.3.2- Kinetic Studies

Kinetic and equilibrium experiments were carried out using the batch equilibrium technique. To each of a set of 5 g sodium form of insolubilized humic acid (INaA) samples placed in tubes, 7.5 ml of cesium solution (prepared from CsCl salt) containing an appropriate amount of ^{137}Cs radiotracer was added. The initial concentration of the solution was $1x10^{-4}$ M. The samples were shaken in a temperature-controlled shaking water bath at room temperature for periods ranging from 5 minutes to 48 hours at 200 rpm. They were centrifuged and 2.5 ml portions of the liquid phases were counted to determine their activities. The same procedure was applied for barium sorption studies using 10 mg INaA and 9 ml of Ba^{2+} solution (prepared from $BaCl_2$ salt) having an appropriate amount of ^{133}Ba radiotracer. When iron nanoparticles were used as a sorbent, 100 mg of sorbent and 10 ml of Ba^{2+} solution with the same initial concentration were shaken at room temperature from 5 minutes to 24 hours. Resulting solutions were centrifuged and 4 ml portions of the liquid phases were counted.

During phenol sorption studies to surfactant modified insolubilized humic acid (SMIA), in order to evaluate kinetic data, separate tubes containing 50 mg SMIA and 8 ml of 20 mgL^{-1} phenol solution were prepared. The samples were shaken at room temperature for periods ranging from 1 hour to 72 hours. After centrifugation, absorbance measurements of liquid phases were carried out at 270 nm using UV-VIS spectrophotometer. Absorbance data were converted into concentration using calibration relations pre-determined at the wavelength of maximum absorbance for each phenol sample.

2.3.3- Effect of Loading, Temperature and pH

Loading experiments were carried out to investigate the effect of initial cation concentrations on sorption at four different temperatures; 15°C, 25°C, 35°C, 45°C and at the initial concetrations of $1x10^{-2}$,$5x10^{-4}$,$1x10^{-4}$,$1x10^{-5}$,$5x10^{-6}$ (mmol/ml) for Cs^{+} sorption onto INaA. In the case of Ba^{2+} sorption onto INaA, the temperature range was between 25°C and 55°C. Concentrations used were $1x10^{-4}$, $1x10^{-5}$,$5x10^{-6}$,$1x10^{-6}$ (mmol/ml). For the study of Ba^{2+} sorption onto iron nanoparticles, the same procedure was applied as above with the initial concentrations of $1x10^{-3}$, $5x10^{-4}$, $1x10^{-4}$, $1x10^{-5}$, $1x10^{-6}$ (mmol/ml) at 25°C and 55°C. Samples were prepared as in the case of kinetic experiments, but all concentrations were used instead of only $1x10^{-4}$ M. The effect of pH upon sorption of Ba^{2+} onto INaA was investigated at a fixed concentration of $1x10^{-5}$ M and room temperature with varying pH values ranging from 1.5 to 8. The samples were shaken, centrifuged and portions of the liquid phase were counted. Shaking was done in a temperature controlled environment using a Nuve ST 402 water bath shaker equipped with microprocessor thermostat. The fluctuation in controlled temperature was ± 1°C.

In the case of phenol sorption onto SMIA, at 25°C adsorption isotherm experiment, the same amount of sorbent and sorbate (as given in the kinetic part) were used in the concentration range from $20mgL^{-1}$ to $80mgL^{-1}$. The solution and sorbent were separated by centrifugation and analyzed for determining the remaining concentration of phenol in solution using UV–Visible spectrophotometer at 270 nm.

To compare the sorption behavior of SMIA with INaA towards cations, sorption behavior of cesium onto SMIA was studied at the initial concetrations of $5x10^{-4}$, $1x10^{-4}$, $1x10^{-5}$, $5x10^{-6}$ (mmol/ml) at 25ºC.

2.4 Spectroscopic Characterization of Humic Acid, Its Modified Forms and Iron Nanoparticles and Analysis of Phenol Solutions

2.4.1 Fourier Transform Infrared Spectroscopy

FT-IR spectra were recorded using a Bruker Tensor 27 FTIR spectrometer with a standard high sensitivity DLATGS detector, with a resolution of 4 cm^{-1} and 64 scans, The KBr pellets were obtained by pressing a mixture of 1:100 ratio of humic acid samples and KBr, respectively.

2.4.2 ^{13}C CP/MAS Nuclear Magnetic Resonance Spectroscopy

Solid-state ^{13}C NMR spectra were obtained at the ^{13}C resonance frequency of 125.721 MHz on a Bruker Avance ASX 500 spectrometer, equipped with a double resonance HX probe**.**The samples were confined in a zirconium oxide rotor with an external diameter of 2.5 mm**.** The Cross-Polarization Magic Angle Spinning CPMAS technique was applied with a contact time of 1 ms, a spinning speed of 15 kHz MAS and a pulse delay of 2 s.

2.4.3 Powder X-Ray Diffraction

To examine the effect of barium solution on iron nanoparticle surface, XRD technique was used. The XRD patterns were obtained on a Rigaku Miniflex diffractometer using a high-power Cu Kά source operating at 30 kV/15 mA.

2.4.4 UV-Visible Spectrophotometer

UV-Vis spectra were recorded using a Varian Cary 5 double beam spectrophotometer over a wavelength range between 300 and 200 nm in absorbance mode with 100 nm min^{-1} speed.

2.4.5 Scanning Electron Microscope

The iron nanoparticle samples were analyzed using a Philips XL-30S FEG type SEM/EDS instrument at different magnifications.

3. RESULTS AND DISCUSSIONS

3.1- Characterization of Sorbents

Fourier transform infrared (FTIR) and solid state ^{13}C MAS-NMR and spectroscopic techniques were used to study the structural changes during humic acid (HA) modification. Potantiometric titration method was used to determine acidic functional groups of humic acid quantitatively. Iron nanoparticles were characterized using powder X-ray diffraction (PXRD) and scanning electron microscope (SEM) techniques.

3.1.1- Potantiometric Titration

To quantify the acidic functional (carboxylic and phenolic) groups, potantiometric titration method was used. It is usual to plot the differential curves, $\Delta pH / \Delta V$ or $\Delta E / \Delta V$ against volume of titrant added, but when the titration curve is not symmetrical about the equivalence point, as in our case shown in Fig. 3.1, it is possible to obtain erroneous results. Therefore, G.Gran[22] developed mathematical expressions to linearize various titration curves. In our data treatment, we chose the following equation, assuming humic acid as a polymeric acid and titration type as weak acid-strong base titration.

$$\text{Gran Function (G)} = V \times 10^{pH - k} \qquad (1)$$

Where V represents the amount of titrant used (ml) and k is an arbitrary constant with a value such that the Gran function value will fall in a suitable range such as 0 to 100-1000.

After conversion of the potantiometric titration data to linearized form using Gran functions, two associated lines were obtained as shown in Fig. 3.2. The intersection of the first line gives the amount of base needed to neutralize carboxylic acid groups and the second intersection point is the amount of total base

which is required to neutralize all acidic functional groups. The difference is the amount of base which is required to neutralize phenolic groups. The following quantitative acidic functional group and total acidity values obtained are given in Table 3.1.

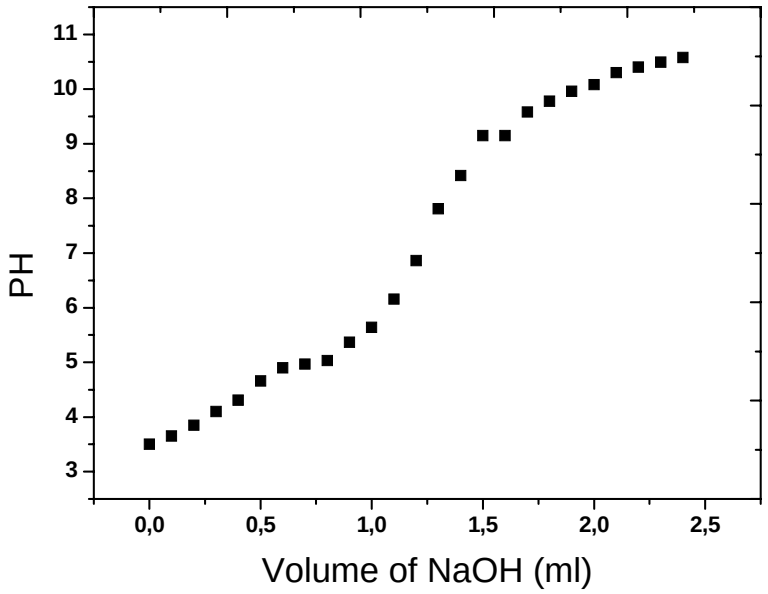

Fig. 3.1: Potantiometric titration curve of humic acid used in our experiment

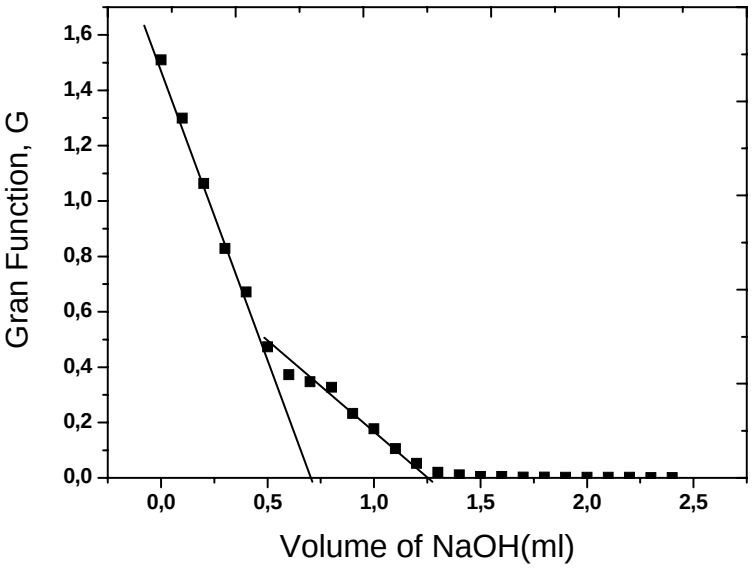

Fig. 3.2: Linearized plot potantiometric titration curve of humic acid using Gran function.

Table 3.1. Acidic functional group contents obtained experimentally using potantiometric titration (meq/100g) of humic acid.

-COOH	$-C_6H_5OH$	Total Acidity
249.0	190.0	439.0

3.1.2- Characterization of Humic acid and Its Modified Forms

FTIR spectroscopic technique was used to examine the structural changes after insolubilization of humic acid. The peaks and corresponding functional groups in FTIR spectra shown in Fig.3.3 are as follows; a broad band at 3387 cm^{-1} primarily corresponds to O-H strectching and secondarily to N-H stretching, the peak at 3071 cm^{-1} represents stretching of aromatic C-H, absorption bands at 2928 and 2857 cm^{-1} are attributed to aliphatic C–H stretching in CH_2 and CH_3, respectively, Broad bands at 2500 cm^{-1} is overtone from carboxylic groups stretching (2 x 1246 cm^{-1}) and at 2000 cm^{-1} is overtone from C–O polysaccharides stretching mode (2 x 1060 cm^{-1}), Strong absorption band at 1704 cm^{-1} is due to C=O stretching of carboxylic acid and ketone. Absorption bands at 1602 cm^{-1} and 1372 cm^{-1} are ascribed to stretching of carboxylate ion and the peak at 1602 cm^{-1} can also be attributed to structural vibrations of aromatic C=C bonds , the peak at 1222 cm^{-1} represents C-O stretching in phenols and O–H deformation of COOH. Absorptions from deformation of aliphatic C–H and, H-bonded C=O of conjugated ketones occurs at 1448 cm^{-1}, the band at 1033 cm^{-1} represents C-O stretching of polysaccharides[23,24,25].

The ^{13}C spectra of humic acid (HA) and insolubilized humic acid (INaA) shown in Fig. 3.4 include following peaks: alkyl carbons and *O*-alkyl carbons (aminoacids and carbons adjacent to ester/ether/hydroxyl) (0-60ppm), because that peak was not well resolved we observe those two groups in a broad band; (110-145) ppm is assigned to aromatic carbon, the peak at (150-190) ppm include phenolic and carboxylic carbons[26,27,28].

When we examine FTIR and ^{13}C NMR spectra of HA and INaA, we observe that there is a decrease at the intensities of aliphatic alkyl groups, -COOH group and phenolic groups, the effect causing insolubilization is mainly due to loss in carboxyl groups, but as we see on spectrum, all of the adsorption sites are not lost during insolubilization. In the literature[16], it was found by titration methods that the lost in percentage of acidic functional groups is nearly 25%. By this way, the ability of HA to make hydrogen bonding decreased and that caused the insolubilization of HA in water at high pH values. It is also clear from the ^{13}C NMR spectra that aromatic part of HA is not affected during insolubilization process, because there is no intensity change.

Insolubilized humic acid showed no tendency to adsorb phenol molecules. Therefore, we modified sodium form of insolubilized humic acid with cationic surfactant (cetyltrimethylammoniumchloride) by making its surface nonpolar to ensure the adsorption of phenol. After modification, alkyl peaks appeared at 2928 and 2857 cm^{-1} on FTIR spectrum of surfactant modified insolubilized humic acid (SMIA) as shown in Fig. 3.5.

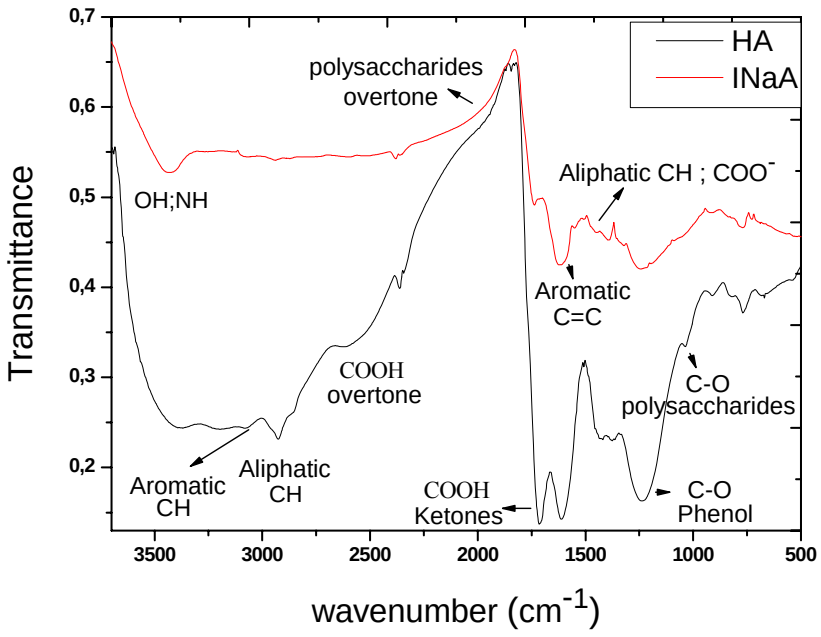

Fig. 3.3: FTIR spectra of humic acid and sodium form of insolubilized humic acid.

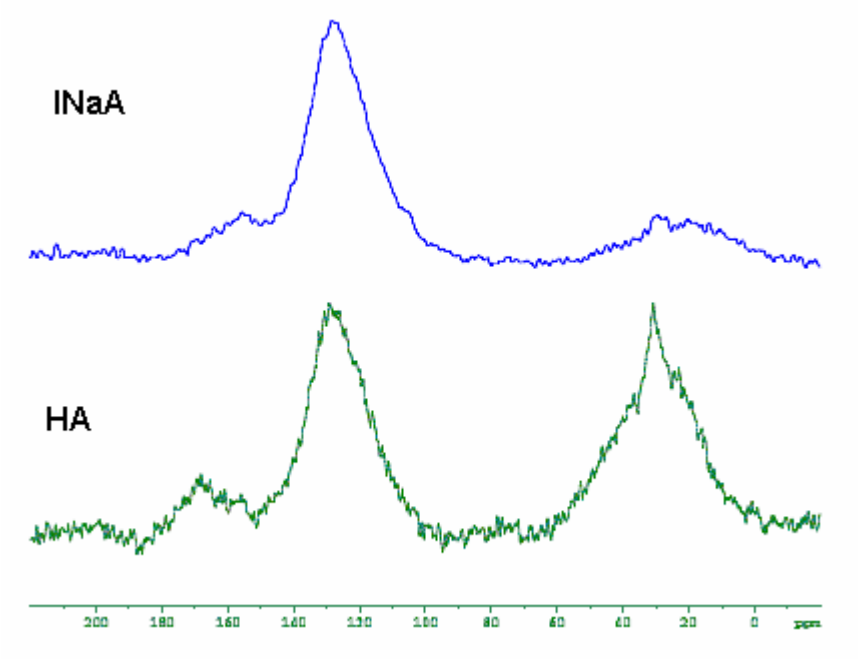

Fig. 3.4: ^{13}C NMR spectra of humic acid and sodium form of insolubilized humic acid.

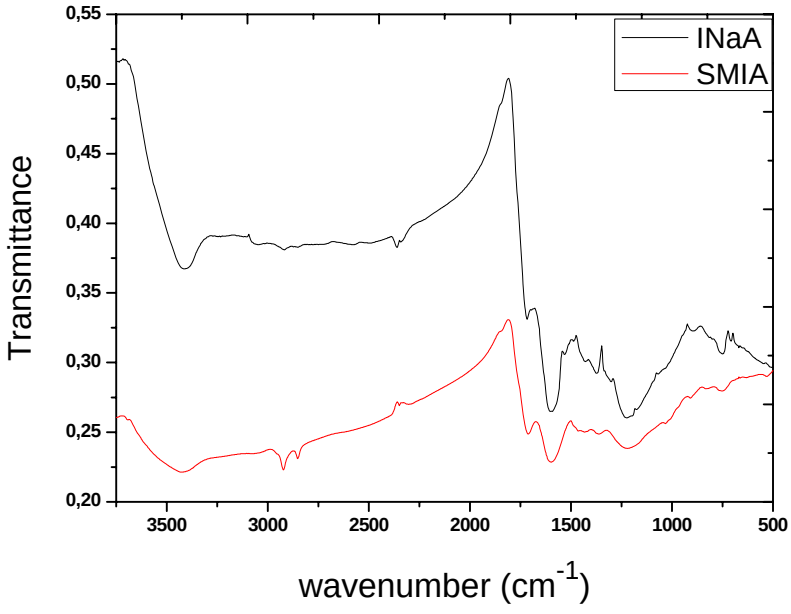

Fig. 3.5: FTIR spectra of sodium form of insolubilized humic acid and surfactant modified insolubilized humic acid

3.1.3- Characterization of Iron Nanoparticles

Particle shape, size and composition are important properties that affect the chemical and physical properties of nanoparticles. To provide primary characterization of these properties, XRD pattern (Fig. 3.6) and SEM images at different magnifications (Fig. 3.7) were obtained for iron nanoparticles (nano-Fe^0). XRD pattern for nano-Fe^0 yielded a broad peak for α-Fe^0 (ferrite-BCC crystal structure) with mean crystallite dimensions <1.5nm. This broadening of diffraction peak suggests a distribution of crystallite dimensions[18]. These small crystals are aggregated into spherical <100nm particles, and these particles are further aggregated into the chains as shown in Fig. 3.7. The size of particles and the observation of chain structure of iron nanoparticles are in agreement with previous studies[29,30]. After mixing nano-Fe^0 with aqueous barium solution, some more peaks appeared on XRD pattern, because nano-Fe^0 are surrounded by an oxide shell which are iron oxides with different crystal structures. The oxide layer is formed by the oxidation of Fe^0 nanoparticles.

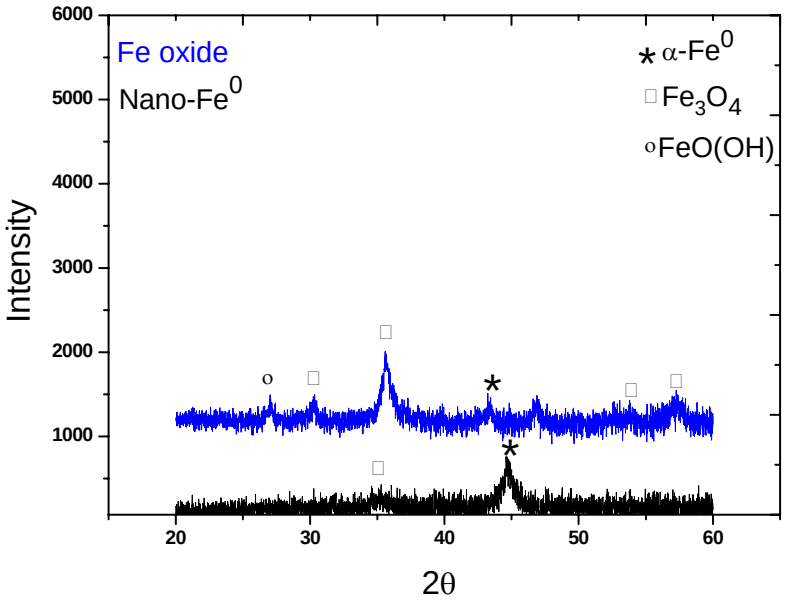

Fig. 3.6: XRD Pattern for nano-Fe^0 and its oxide form

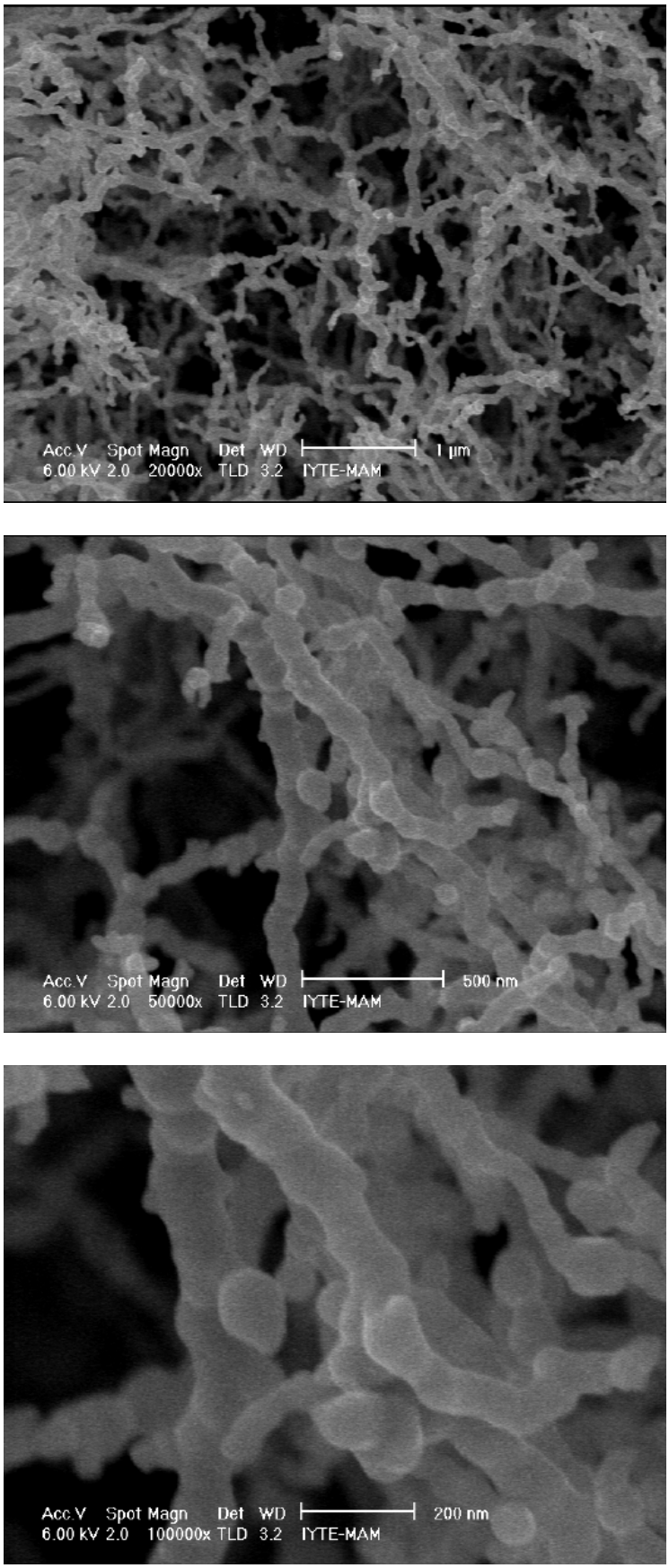

Fig. 3.7 SEM images of iron nanoparticles at 1µm, 500nm and 200nm magnifications

3.2- Radiochemical Sorption Studies

3.2.1- Kinetic Studies

The experimental data in adsorption are expressed in terms of the ditribution ratio, R_d, defined as the ratio of adsorbate concentration on solid phase to its concentration in liquid phase. The distribution ratio of adsorption is defined as :

$$R_d = \frac{[C]_s}{[C]_l} \qquad (2)$$

Where $[C]_s$ (mmol/g) and $[C]_l$ (mmol/ml) are the concentrations of species C in the solid and liquid phases, respectively. At the beginning of the sorption step, V (ml) of solution with initial concentration [C]° (mmol/ml) is used and at the end of the sorption step V (ml) of solution with concentration $[C]_l$ are present, hence the concentration of C in the solid phase after sorption can be expressed as:

$$[C]_s = \frac{V([C]° - [C]_l)}{W_s} \qquad (3)$$

In terms of radiactivity, $[C]_l$ can be written as:

$$[C]_l = \frac{A_l}{A°}[C]° \qquad (4)$$

From (2)-(4), the following equation is obtained:

$$R_d = \frac{VA° - VA_l}{A_l W_s} \qquad (5)$$

Where A° is the initial count rate of solution added for sorption (cps)/ml, A_l is the count rate of solution after sorption (cps)/ml, W_s is the weight of solid material (g)[31].

The sorption kinetics of Cs^{+} and Ba^{2+} ions on INaA (sodium form of insolubilized humic acid) and Ba^{2+} ion on iron nanoparticles were examined by radioactive tracer method to determine the time required to reach equilibrium, rate constants and the nature of the kinetic model for each sorption process. The results of the variation of R_d as a function of time for Cs^{+} and Ba^{2+} ions on INaA and iron nanoparticles are given in Fig. 3.8, 3.9, 3.10 and in Tables 3.2, 3.3 and 3.4.

It is apparent that, equlibrium is reached after several hours of contact in each process. Such a rapid process indicates that sorption is primarily a surface phenomenon where the humic acid and iron nanoparticle surfaces are readily accessible to ions in solution. On the basis of the obtained results an equilibrium period of 24 hours were selected as a fixed parameter for further experiments, where the effects of loading and temperature, were examined when INaA was used as a sorbent. In the case of iron nanoparticles as a sorbent, 5 hours were selected as an equilibrum time.

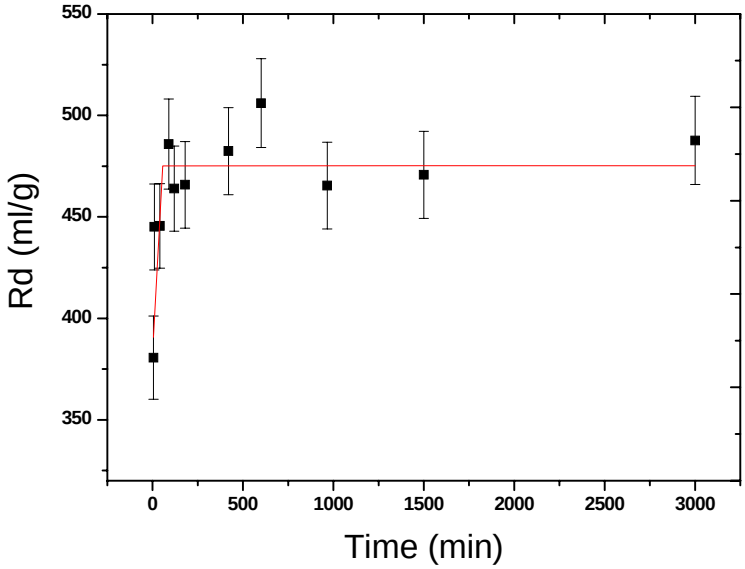

Fig. 3.8: Variation of R_d values with shaking time for Cs^{+} sorption onto sodium form of insolubilized humic acid at an initial concentration of $1x10^{-4}$M at 25°C

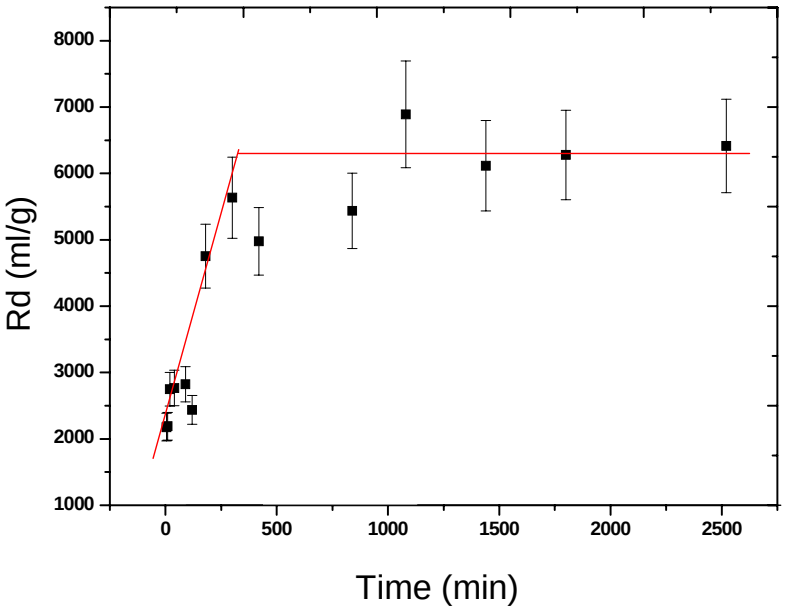

Fig. 3.9: Variation of R_d values with shaking time for Ba^{2+} sorption onto sodium form of insolubilized humic acid at an initial concentration of $1x10^{-4}$M at 25°C

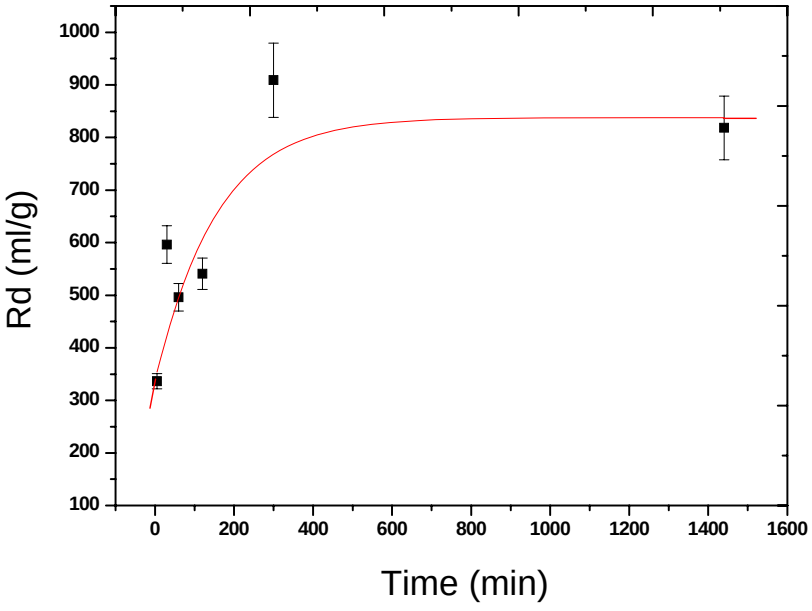

Fig. 3.10: Variation of R_d values with shaking time for Ba^{2+} sorption on iron nanoparticles at an initial concentration of 100mg/L at 25°C

Table 3.2: The sorption data for the kinetic behavior Cs^+ ion onto sodium form of insolubilized humic acid at an initial concentration of $1x10^{-4}$M.

Time (min)	Rd (ml/g)	$[Cs]_{liq}$ (mmol/ml)	$[Cs]_s$ (mmol/g)	t/q
5	381	$6,63 \times 10^{-5}$	0,0252	198
10	445	$6,27 \times 10^{-5}$	0,0279	358
40	446	$6,27 \times 10^{-5}$	0,0279	1431
90	486	$6,07 \times 10^{-5}$	0,0295	3052
120	464	$6,18 \times 10^{-5}$	0,0287	4186
180	466	$6,17 \times 10^{-5}$	0,0287	6264
420	482	$6,08 \times 10^{-5}$	0,0294	14306
600	506	$5,97 \times 10^{-5}$	0,0302	19857
966	465	$6,17 \times 10^{-5}$	0,0287	33634
1500	471	$6,14 \times 10^{-5}$	0,0289	51869
3000	488	$6,06 \times 10^{-5}$	0,0295	101514

Table 3.3: The sorption data for the kinetic behavior Ba^{2+} ion on sodium form of insolubilized humic acid at an initial concentration of $1x10^{-4}$M.

Time (min)	Rd (ml/g)	$[Ba]_{liq}$ (mmol/ml)	$[Ba]_s$ (mmol/g)	t/q
5	2177	$4,53 \times 10^{-5}$	0,0985	51
10	2190	$4,51 \times 10^{-5}$	0,0988	101
20	2749	$3,96 \times 10^{-5}$	0,1088	184
40	2766	$3,94 \times 10^{-5}$	0,1090	367
90	2825	$3,89 \times 10^{-5}$	0,1099	818
120	2439	$4,25 \times 10^{-5}$	0,1036	1159
180	4755	$2,75 \times 10^{-5}$	0,1306	1378
300	5636	$2,42 \times 10^{-5}$	0,1364	2199
420	4978	$2,66 \times 10^{-5}$	0,1322	3177
840	5436	$2,49 \times 10^{-5}$	0,1352	6212
1080	6890	$2,07 \times 10^{-5}$	0,1427	7567
1440	6116	$2,27 \times 10^{-5}$	0,1391	10354
1800	6280	$2,23 \times 10^{-5}$	0,1399	12866
2520	6415	$2,19 \times 10^{-5}$	0,1406	17928

Table 3.4: The sorption data for the kinetic behavior of Ba^{2+} ion onto iron nanoparticles at an initial concentration of 100mg/L.

Time (min)	**Rd (ml/g)**	**$[Ba]_{liq}$ (mmol/ml)**	**$[Ba]_s$ (mmol/g)**	**t/q**
5	336	$2,29 \times 10^{-5}$	0,00771	649
30	596	$1,44 \times 10^{-5}$	0,00856	3503
60	496	$1,68 \times 10^{-5}$	0,00832	7210
120	541	$1,56 \times 10^{-5}$	0,00844	14219
300	909	$9,91 \times 10^{-5}$	0,00901	33301
1440	818	$10,89 \times 10^{-5}$	0,00891	161598

Kinetic studies were also used to determine the most suitable rate equations and rate constants of cation sorption. Correlation coefficient values indicate that pseudo second order rate equation[32] describe the sorption behavior of cesium and barium ions onto INaA and barium ions onto iron nanoparticles, quite well.

The rate law for this system is expressed as:

$$\frac{dq}{dt} = k_2 (q_e - q)^2 \qquad (6)$$

where q and q_e are the amount of solute sorbed per gram of sorbent at any time t, and at equilibrium, respectively, and k_2 is the pseudo second order rate constant of sorption. After integration and rearrangement of the above equation, the following equation is obtained in linear form,

$$\frac{t}{q} = \frac{1}{k_2 q_e^2} + \frac{1}{q_e} t \qquad (7)$$

The plot of t/q versus t gives a straigt line with slope of $1/q_e$ and intercept of $1/k_2 q_e^2$. So the amount of cation sorbed per gram of sorbent at equilibrium q_e and sorption rate constant k_2 could be evaluated from the slope and intercept, respectively.

The results are shown in Fig. 3.11, 3.12, 3.13 and in Table 3.5. It is apparent from q_e values that barium ions are sorbed by INaA five times more than cesium ions. Barium ions have less tendency to be adsorbed onto iron nanoparticles when compared to sorption onto INaA. The sorption order with ion-sorbent pair is barium-INaA > cesium-INaA > barium-iron nanoparticles. The reason for the less sorption tendency of cesium ions onto INaA can be explained by their charge. An increase in the oxidation state favors the accumulation of the ion on the sorption surface leading to electrostatic stability. The low sorption behavior of barium onto iron nanoparticles can be explained by comparing surface properties of INaA and iron nanoparticles. Humic acid is the combination of many small organic molecules with many carboxylic acid and phenolic hydroxly groups. These functional groups are primarily distributed on the surface. These functional groups are highly polar. In its modified form, INaA, the acidic hydrogens bonded to oxygen atoms were exchanged with sodium ions and this made those functional groups negatively charged. As a result carboxylic acid and phenolic groups became carboxylate and phenolate ions having higher polarity which increases the cation sorption affinity. When iron nanoparticles contact water molecules, the surface is covered by the oxide layer and this layer is responsible for the sorption behavior of iron nanoparticles toward cations. When we compare the surface of iron nanoparticles with INaA, it is obvious that INaA surface is covered with negatively charged oxygen groups which give the surface higher sorption capacity than the iron nanoparticle surface having oxide layers.

The rate constant values of the three sorption cases studied have an inverse relationship with sorption affinity. The order for the rate of sorption with ion-sorbent pairs is as the following; barium-iron nanoparticles > cesium-INaA > barium-INaA.

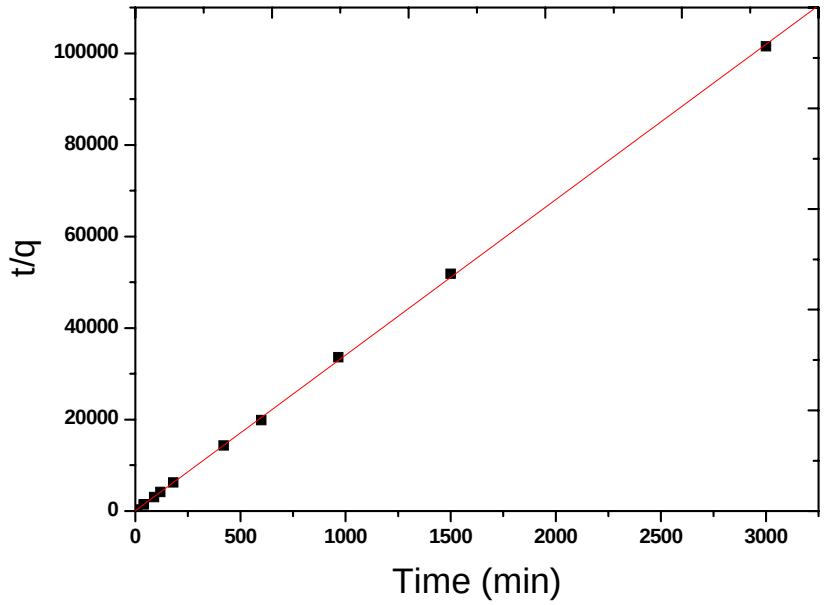

Fig. 3.11: Variation of t/q Values with Shaking time for Cs^{+} sorption on sodium form of insolubilized humic acid at 25°C

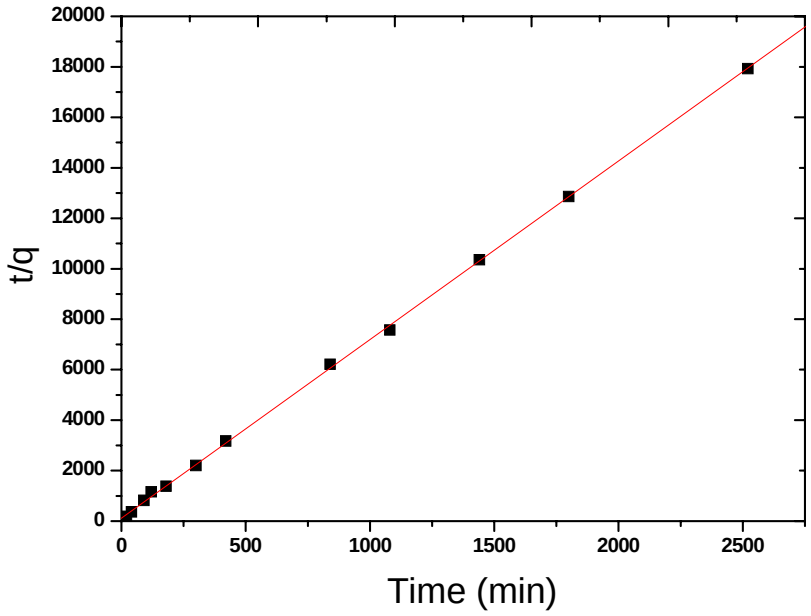

Fig. 3.12: Variation of t/q Values with Shaking time for Ba^{2+} sorption on sodium form of insolubilized humic acid at 25°C

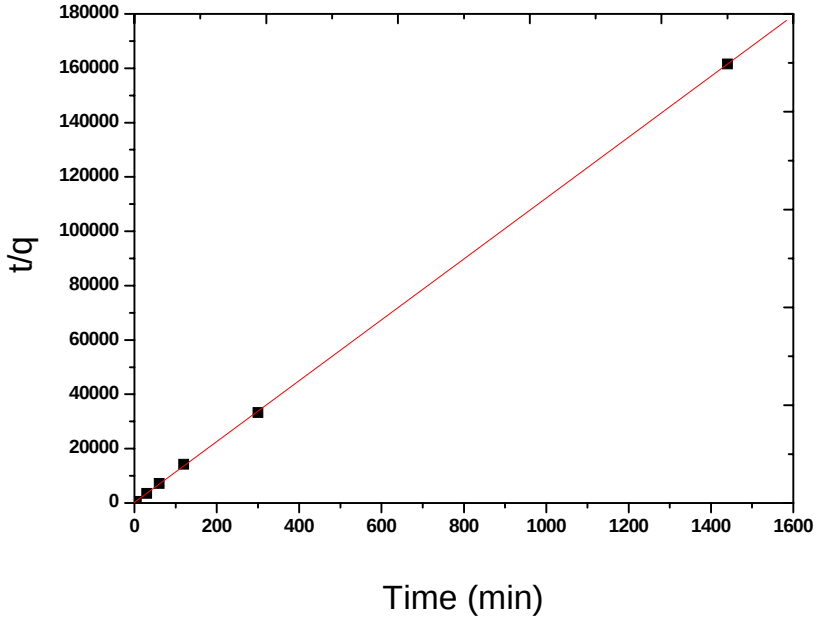

Fig. 3.13: Variation of t/q Values with Shaking time for Ba^{2+} sorption on iron nanoparticles at 25°C

Table 3.5 : Amount of sorbed cation per gram of sorbent, pseudo second order rate constants and correlation coefficient values for cesium and barium sorption

Sorbents	**Sorbed Cation**	**q_e (mol/g)**	**k_2 ($g.mol^{-1}.min^{-1}$)**	**R^2**
INaA	Cs^+	29.44×10^{-3}	9.998	0.9998
INaA	Ba^{2+}	141.30×10^{-3}	0.432	0.9997
Nano-Fe^0	Ba^{2+}	8.93×10^{-3}	49.600	1.0000

3.2.2- Loading and Temperature Studies

3.2.2.1- Loading Curves

Loading experiments were carried out to investigate the effect of initial concentration on sorption. The loading curves were constructed by plotting log R_d values against log $[C]_{s,}$ at four different temperatures. The results are shown in Figs. 3.14, 3.15, 3.16, 3.17 for cesium and barium ion sorptions onto INaA and barium sorption on iron nanoparticles. Sorption data of Cs^+ and Ba^{2+} onto INaA and Ba^{2+} onto iron nanoparticles at different initial cation concentrations and temperatures are given in Tables 3.6, 3.7, 3.8.

It is clear from the Tables 3.6, 3.7, 3.8 that as the initial concentration increases, the R_d values decrease in all cases. This arises, because as the initial concentration of the sorbed cation is increased, the ratio of the ions that are accommodated by the solid surface to those remaining in solution decreases since a limited number of sites on INaA and iron nanoparticle surfaces are available for sorption.

The loading curves indicate that the Cs^+ and Ba^{2+} sorption onto INaA show similar shapes, indicating that the sorption occurs on single sorption site. This sorption site is negatively charged oxygen atoms belonging to carboxylate and phenolate groups on INaA. Temperature change between 25°C and 55°C did not significantly change the shape of these curves, indicating that these functional groups are stable and are not affected in this temperature range. In the case of Ba^{2+} sorption onto iron nanoparticles between the same temperature range, it is shown that single site is responsible for barium sorption. The sorption site on iron nanoparticles is the iron oxides which are mainly magnetite (Fe_3O_4) and ironoxyhydroxide (FeO(OH)).

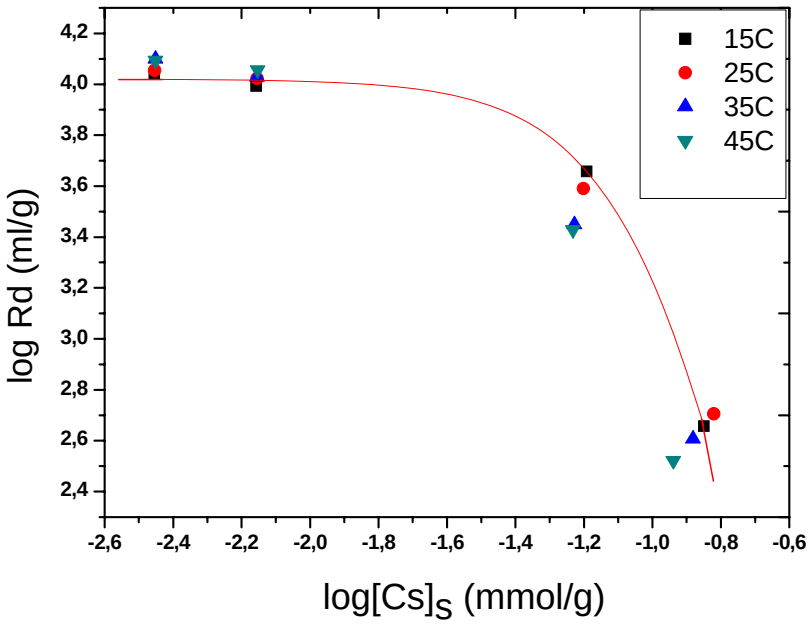

Fig.3.14: The loading curves for sorption of Cs^{+} onto sodium form of insolubilized humic acid at different temperatures

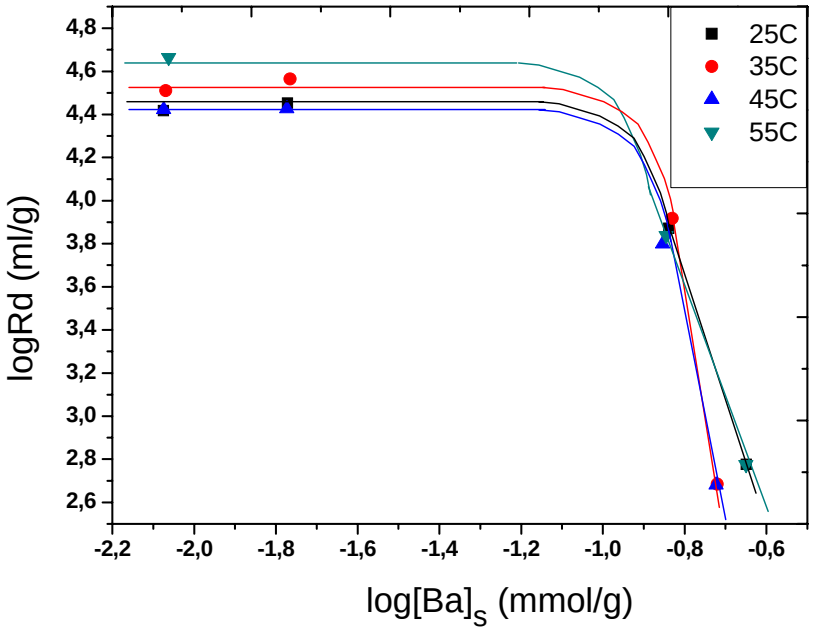

Fig.3.15: The loading curves for sorption of Ba^{2+} onto sodium form of insolubilized humic acid at different temperatures

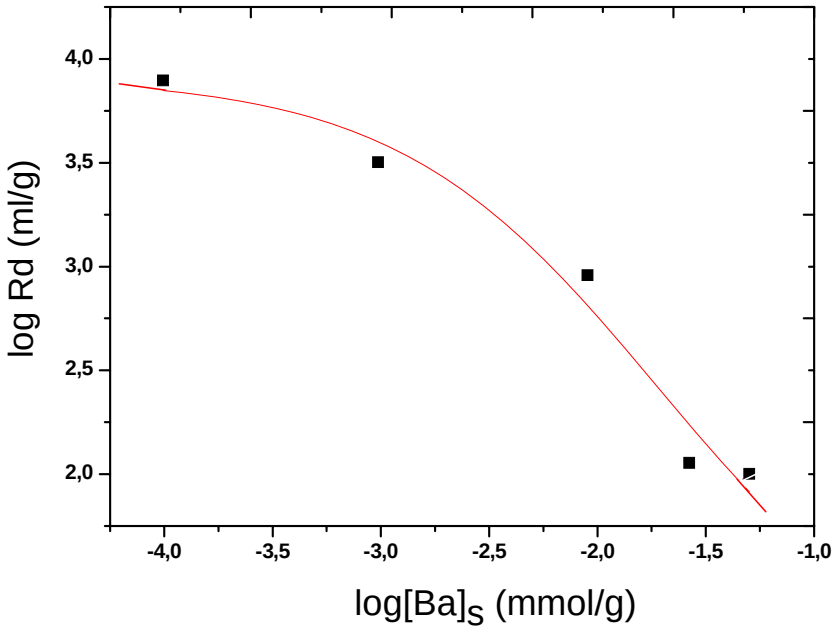

Fig.3.16: The loading curve for sorption of Ba^{2+} onto iron nanoparticles at 25°C

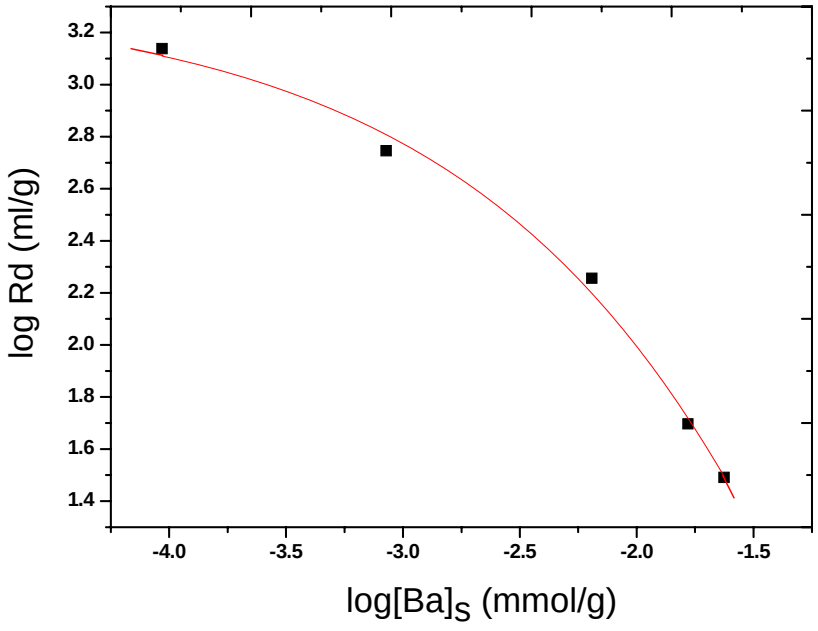

Fig.3.17: The loading curve for sorption of Ba^{2+} onto iron nanoparticles at 55°C

Table 3.6: The data of Cs^+ sorption onto sodium form of insolubilized humic acid at different temperatures and initial concentrations.

Temp(K)	[C]°(mmol/ml)	R_d (ml/g)	$[Cs]_s$ (mmol/g)	$[Cs]_{liq}$ (mmol/ml)
288	**$1x10^{-2}$**	**48**	**0,449**	**$9.4x10^{-3}$**
288	$5x10^{-4}$	454	0,141	$3,11x10^{-4}$
288	$1x10^{-4}$	4548	0,0644	$1,41\ x10^{-5}$
288	$1x10^{-5}$	9849	0,00697	$7,08\ x10^{-7}$
288	$5x10^{-6}$	10984	0,00351	$3,20\ x10^{-7}$
298	**$1x10^{-2}$**	**119**	**1,028**	**$8.63x10^{-3}$**
298	$5x10^{-4}$	507	0,151	$2,98\ x10^{-4}$
298	$1x10^{-4}$	3894	0,0629	$1,61\ x10^{-5}$
298	$1x10^{-5}$	10554	0,00700	$6,63\ x10^{-7}$
298	$5x10^{-6}$	11343	0,00352	$3,10\ x10^{-7}$
308	**$1x10^{-2}$**	**52**	**0,491**	**$9.35x10^{-3}$**
308	$5x10^{-4}$	405	0,131	$3,25\ x10^{-4}$
308	$1x10^{-4}$	2810	0,0592	$2,11\ x10^{-5}$
308	$1x10^{-5}$	10693	0,00701	$6,55\ x10^{-7}$
308	$5x10^{-6}$	12591	0,00354	$2,81\ x10^{-7}$
318	**$1x10^{-2}$**	**42**	**0,398**	**$9.47x10^{-3}$**
318	$5x10^{-4}$	332	0,115	$3,46\ x10^{-4}$
318	$1x10^{-4}$	2675	0,0586	$2,19\ x10^{-5}$
318	$1x10^{-5}$	11372	0,00704	$6,19\ x10^{-7}$
318	$5x10^{-6}$	12416	0,00354	$2,85\ x10^{-7}$

Table 3.7: The data of Ba^{2+} sorption onto sodium form of insolubilized humic acid at different temperatures and initial concentrations.

Temp(K)	[C]° (mmol/ml)	R_d(ml/g)	$[Ba]_s$(mmol/g)	$[Ba]_{liq}$(mmol/ml)
298	**$1x10^{-4}$**	**7446**	**0,145**	**$1,95x10^{-5}$**
298	$1x10^{-5}$	18065	0,0164	$9,06x10^{-7}$
298	$5x10^{-6}$	26153	0.00842	$3,22x10^{-7}$
298	$1x10^{-6}$	58874	0,00175	$2,97x10^{-8}$
308	**$1x10^{-4}$**	**8275**	**0,148**	**$1,79\ x10^{-5}$**
308	$1x10^{-5}$	22938	0,0167	$7,28\ x10^{-7}$
308	$5x10^{-6}$	32368	0,00853	$2,63\ x10^{-7}$
308	$1x10^{-6}$	27026	--	--
318	**$1x10^{-4}$**	**6439**	**0,141**	**$2,18\ x10^{-5}$**
318	$1x10^{-5}$	23292	0,0167	$7,17\ x10^{-7}$
318	$5x10^{-6}$	26522	0,00843	$3,18\ x10^{-7}$
318	$1x10^{-6}$	37487	0,00172	$4,58\ x10^{-8}$
328	**$1x10^{-4}$**	**6896**	**0,143**	**$2,07\ x10^{-5}$**
328	$5x10^{-6}$	38156	0,00859	$2,25\ x10^{-7}$
328	$1x10^{-6}$	43284	0,00173	$3,99x10^{-8}$

Table 3.8: The data of Ba^{2+} sorption onto iron nanoparticles at different temperatures and initial concentrations.

Temp(K), W_s	**Concentration (M)**	**R_d (ml/g)**	**$[Ba]_s$ (mmol/g)**	**$[Ba]_{liq}$ (mmol/ml)**
298, 100mg	**10^{-3}M**	100	0,0501	$4,99 \times 10^{-4}$
298	5×10^{-4}M	113	0,0266	$2,34 \times 10^{-4}$
298	10^{-4}M	909	0,00901	$9,91 \times 10^{-6}$
298	10^{-5}M	3175	$9,695 \times 10^{-4}$	$3,05 \times 10^{-7}$
298	10^{-6}M	7877	$9,875 \times 10^{-5}$	$1,25 \times 10^{-8}$
298, 50mg	**10^{-3}M**	**72**	**0,0531**	**$7,35 \times 10^{-4}$**
298	5×10^{-4}M	102	0,0338	$3,31 \times 10^{-4}$
298	10^{-4}M	459	0,0139	$3,04 \times 10^{-5}$
298	10^{-5}M	4197	0,00191	$4,55 \times 10^{-7}$
298	10^{-6}M	5863	$1,934 \times 10^{-4}$	$3,30 \times 10^{-8}$
298, 25mg	**10^{-3}M**	**67**	**0,0574**	**$8,56 \times 10^{-4}$**
298	5×10^{-4}M	90	0,0367	$4,08 \times 10^{-4}$
298	10^{-4}M	429	0,0207	$4,82 \times 10^{-5}$
298	10^{-6}M	4274	$3,658 \times 10^{-4}$	$8,56 \times 10^{-8}$
328, 100mg	**10^{-3}M**	**31**	**0,0237**	**$7,63 \times 10^{-4}$**
328	5×10^{-4}M	50	0,0166	$3,34 \times 10^{-4}$
328	10^{-4}M	180	0,00643	$3,57 \times 10^{-5}$
328	10^{-5}M	557	$8,479 \times 10^{-4}$	$1,52 \times 10^{-6}$
328	10^{-6}M	1373	$9,321 \times 10^{-5}$	$6,79 \times 10^{-8}$

3.2.2.2- Effect of pH

The increase of pH has a substantial effect upon sorption of Ba^{2+} onto INaA, as shown in Fig. 3.18. The experiment was carried out using 10 mg of INaA as sorbent, 9 ml of $1x10^{-5}$ M of Ba^{2+} solution with varying pH values at 200 rpm. It is seen that there is almost no adsorption between pH 1-2. In aqueous media there is a competition between H_3O^+ and metal ions toward the solid phase. At low pHs, the surface of the adsorbent is closely associated with the hydronium ions and repulsive forces limit the approach of the metal ions. As we increase the pH, we observe a dramatic increase of the uptake of Ba^{2+} by INaA, because of the principal adsorption sites –COOH and –COH dissociate to their anionic forms $–COO^-$ and CO^-. These dissociations cause negatively charged surfaces and cations could more easily adsorb onto the solid surface. At pH value beyond 8, we observe a sharp decrease at sorption capacity of sorbent, because INaA starts to dissolve and adsorbed Ba^{2+} passes from solid phase to solution phase. As a result, adsorption capacity of sorbent (INaA) increases with increasing pH as long as INaA doesn't dissolve.

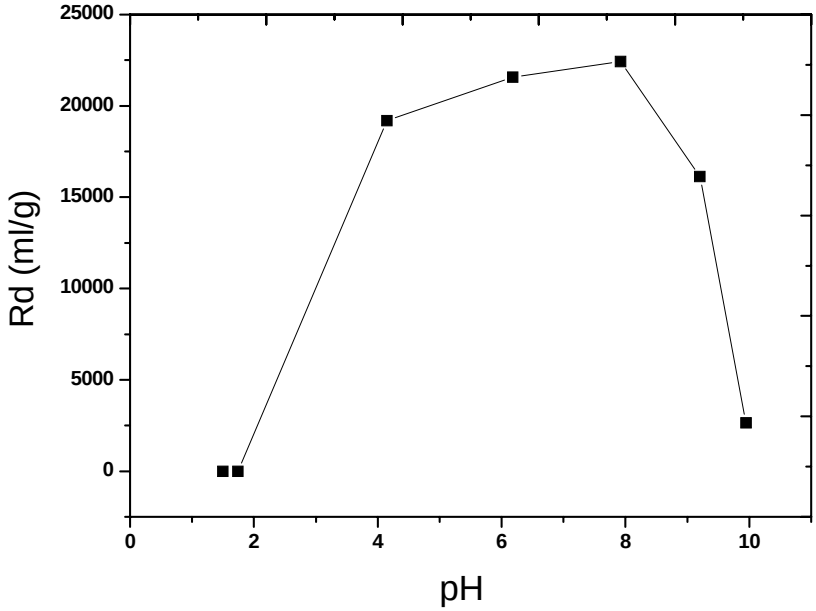

Fig. 3.18 : Effect of pH upon sorption of Ba^{2+} onto sodium form of insolubilized humic acid at 25°C.

3.2.2.3- Freundlich Isotherm

Freundlich isotherm model[20] is one of the most used non-linear model for describing the dependence of sorption on sorbate concentration. This model allows for several kinds of sorption sites on solid and represents properly the sorption data at low and intermediate concentrations on heterogeneous surfaces. The general expression of Freundlich isotherm is given as:

$$[C]_s = k[C]_l^n \qquad (8)$$

Where $[C]_s$ is the amount of ionic species adsorbed on the solid matrix at equilibrium (mmol/g), $[C]_l$ is the concentration of the cation in solution at equilibrium (mmol/ml), *k* and *n*, are Freundlich constants.

This expression can be linearized as:

$$\log [C]_s = \log k + n \log [C]_l \qquad (9)$$

Plotting $\log [C]_s$ versus $\log [C]_l$ yields "n" as the slope and log k as the intercept.

The Freundlich isotherm plots for cesium and barium ions at different loadings and temperatures on INaA and barium ions on iron nanoparticles are given in Figs. 3.19, 3.20, 3.21, 3.22. The Freundlich constants "n" and "k" obtained for different sorption cases are listed in Tables 3.9, 3.10, 3.11.

The values of "n" being less than 1.0 in all cases indicate a non-linear sorption that takes place on a heterogeneous surface. The non-linearity indicates that the sorption energy barrier increases exponentially as the fraction of filled sites on sorbent increases. If we compare the "n" values of Cs^+ and Ba^{2+} ions sorption onto INaA, this is in line with the observed lower R_d values of Cs^+ sorption. When we consider the sorption behavior of these ions onto iron nanoparticles cesium was not sorbed at all, but barium was sorbed because it has a higher charge. An increase

in the oxidation state favors the accumulation of the counter ions on the sorption surface leading to electrostatic stability.

The magnitude of "k" is related to sorption affinity. When we use INaA as a sorbent, we found that there is a significant difference between "k" values for the sorption behavior of cesium and barium ions. This clearly explains that INaA has a much higher tendency to adsorb barium ions compared with cesium ions.

Increase of temperature (40°C) has no pronounced effect on "n" values for the sorption of these cations onto both sorbents, but the "k" values in the case of Ba^{2+} sorption onto INaA has an increasing trend indicating that sorption shows endothermic behavior and for Cs^{+} sorption onto INaA and Ba^{2+} sorption onto iron nanoparticles, it has a decreasing trend which is indicative of exothermic behavior of both sorption processes.

The sorption studies were carried out to examine the effect of mass to volume ratio on the sorption behavior of Ba^{2+} ions onto iron nanoparticles. It was found that there is not a significant effect on the sorption behavior of Ba^{2+} ions onto iron nanoparticles when the mass to volume ratio is changed Figs. (3.22 and 3.26).

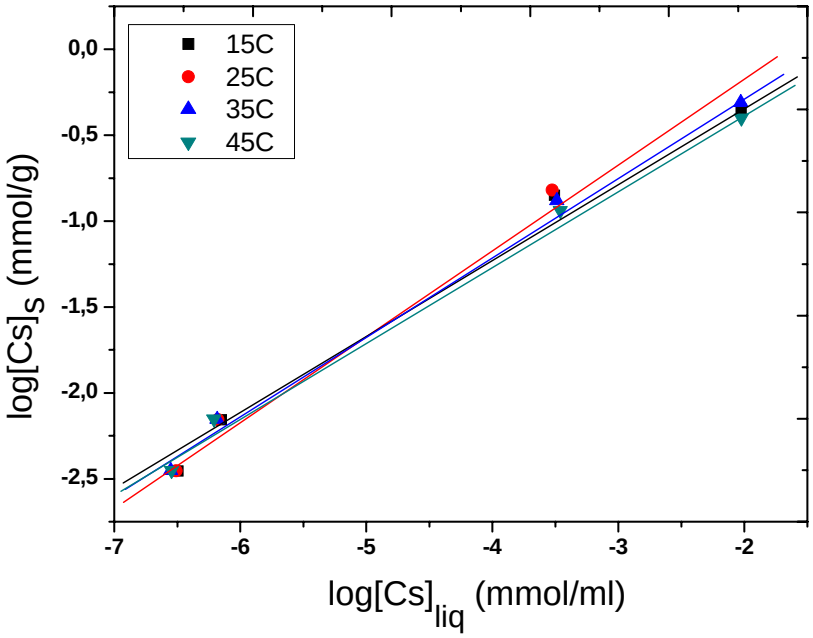

Fig. 3.19: Freundlich isotherm plots for the sorption of Cs^{+} onto sodium form of insolubilized humic acid at various temperatures using 10 mg sorbent.

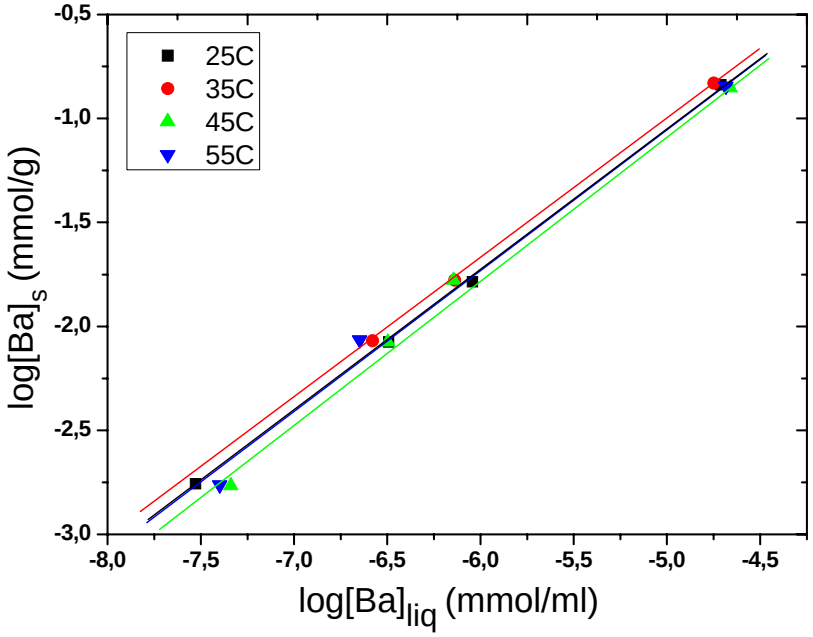

Fig. 3.20: Freundlich isotherm plots for the sorption of Ba^{2+} onto sodium form of insolubilized humic acid at various temperatures using 5 mg sorbent.

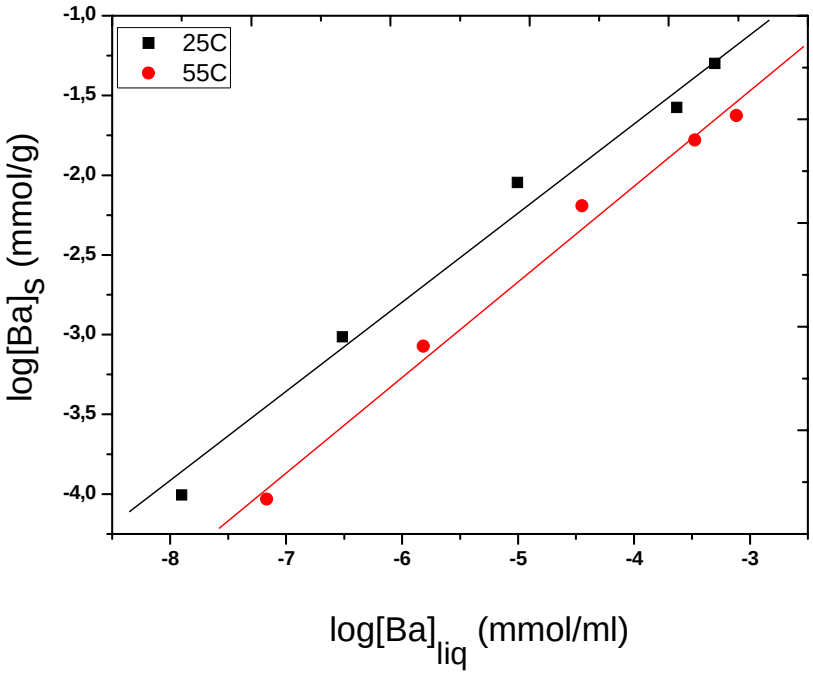

Fig. 3.21: Freundlich isotherm plots for sorption of Ba^{2+} onto iron nanoparticles at 25˚C and 55˚C using 100 mg sorbent.

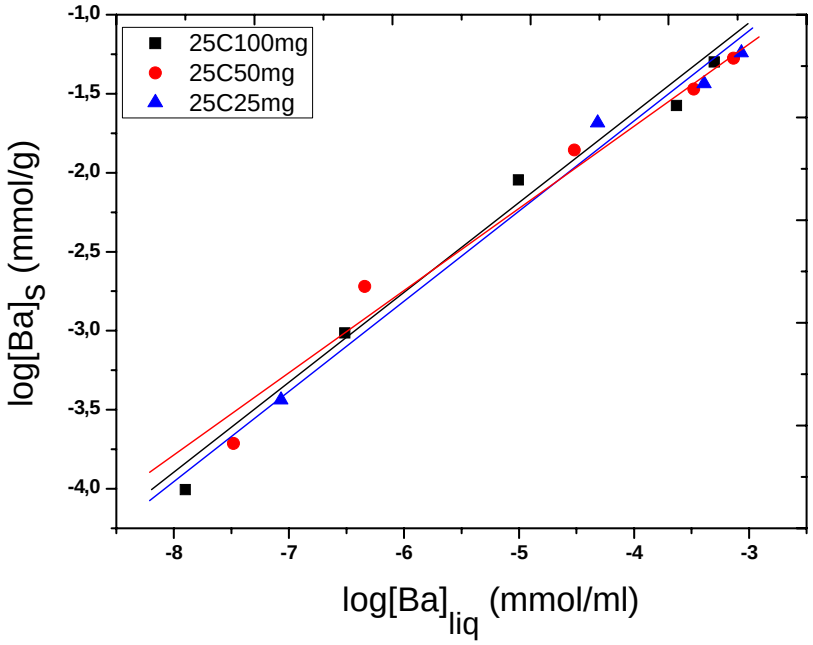

Fig. 3.22: Freundlich isotherm plots for sorption of Ba^{2+} onto iron nanoparticles at 25˚C with different weights 25mg, 50mg and 100mg.

Table 3.9: Freundlich constants , n and k , obtained from the least square fits of the sorption data of Cs^+ onto sodium form of insolubilized humic acid.
(The Linear Correlation Coefficients were all greater than 0,9905)

Sorbed Cation	Freunlich Constant	Temperature (K)			
		288	298	308	318
Cs^+	n	0,4706	0,5305	0,4687	0,4455
	k	4,864	11,405	4,898	3,511

Table 3.10: Freundlich constants , n and k , obtained from the least square fits of the sorption data of Ba^{2+} onto sodium form of insolubilized humic acid.
(The Linear Correlation Coefficients were all greater than 0,9908)

Sorbed Cation	Freundlich Constant	Temperature (K)			
		298	308	318	328
Ba^{2+}	n	0,6814	0,6777	0,7069	0,6891
	k	226,93	243,61	307,26	257,57

Table 3.11: Freundlich constants, n and k, obtained from the least square fits of the sorption data of Ba^{2+} onto iron nanoparticles.
(The linear correlation coefficients were all greater than 0.977)

Sorbed Cation	Freundlich Constant	Temperature (K)	
		298	318
Ba^{+2} (100mg)	n	0.5692	0.5935
	k	4.091	2.052
Ba^{+2} (50mg)	n	0.5329	
	k	2.834	
Ba^{+2} (25mg)	n	0.5504	
	k	3.202	

3.2.2.4- Dubinin-Radushkevich (D-R) Isotherms

The D-R isotherm model[20] is valid at low concetration ranges and can be used to describe sorption on both homogeneous and heterogeneous surfaces. It can be represented by the general expression:

$$[C]_s = C_m \exp-(K\varepsilon^2) \qquad (10)$$

where $[C]_s$ is the amount of ionic species adsorbed on the solid matrix at equilibrium (mmol/g) and C_m is the sorption capacity of adsorbent per unit weight (mmol/g), ε is the polanyi potential, given as RT x $\ln(1+1/[C]_l)$, R is the ideal gas constant (8.3145 J/mol·K), T is the absolute temperature(K), K is a constant related to the energy of sorption. The linear form of the equation above can be obtained by rearranging it to give:

$$\ln [C]_s = \ln C_m - K\varepsilon^2 \qquad (11)$$

If $\ln [C]_s$ is plotted against ε^2, K and $\ln C_m$ will be obtained from the slope and the intercept, respectively. The value of K $(mol/kJ)^2$ is related to the adsorption mean free energy, E (kJ/mol), defined as the free energy change required to transfer one mole of ions from infinity in solution to the solid surface. The relation is given as:

$$E = (2K)^{-1/2} \qquad (12)$$

Sorption on INaA and iron nanoparticles fitted well to the D-R model as shown in Figs. 3.23, 3.24, 3.25 and 3.26. The corresponding values of C_m, K and E found from the fitting of the D-R isotherm model are listed in Tables 3.12, 3.13 and 3.14. The intercept of the D-R isotherm gives information about the maximum adsorption amount and the slope enables the estimation of the adsorption energy which refers to the amount of energy required to transfer one mole sorbed ions from infinity in solution to the solid surface.

C_m values indicate that barium ions are sorbed 5 times more than Cs^+ ions onto INaA and when we compare barium sorption on INaA and iron nanoparticles, we found that barium ions are sorbed 23 times more to the INaA surface. The deprotonated surface functional groups of INaA play a major role for higher cation exchange capacity of INaA.

The affinity of a cation for ion-exchange sites is a function of the charge and size of the cation. For ions of the same charge, we need to consider the hydrated radii which is the effective size of the ion plus its outer covering by water molecules which are tightly bounded by electrostatic attraction. Since the hydrated radius of an ion is inversely proportional to its dehydrated radius[33], the hydrated radius of cesium ion (0.25 nm) is smaller than the hydrated radius of sodium ion (0.40-0.45 nm), consistent with the observed stronger sorption affinity of cesium for ion-exchange sites compared to sodium. Cesium ion sorption results showed lower sorption affinity onto INaA compared to barium ion (0.50 nm), because of the higher charge density of barium leading to stronger sorption complexes.

In all cases, the mean free energy of sorption, E, is in 8-16 kJ/mol energy range corresponding to ion-exchange type of sorption[34].

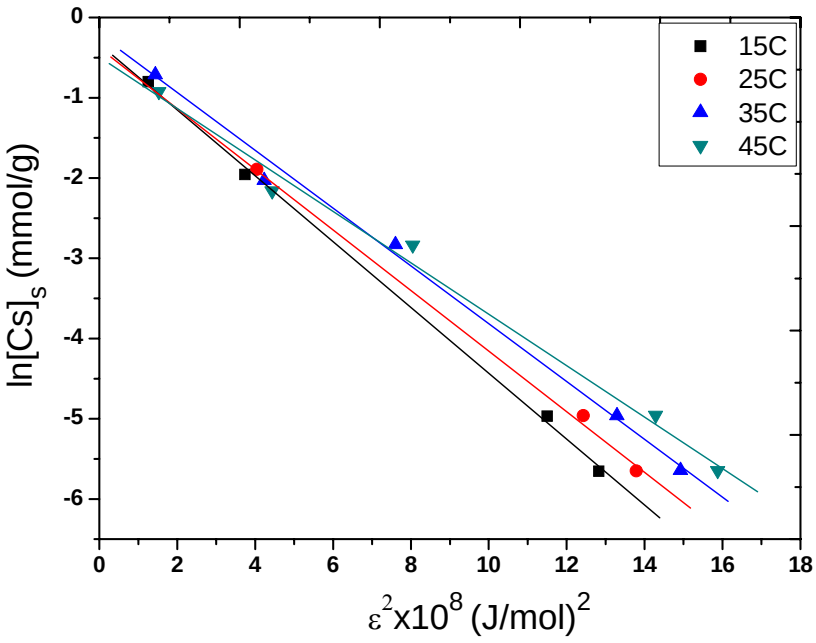

Fig. 3.23: Dubinin-Raduskevich isotherm plots for sorption of Cs^{+} onto sodium form of insolubilized humic acid at various temperatures using 10 mg sorbent.

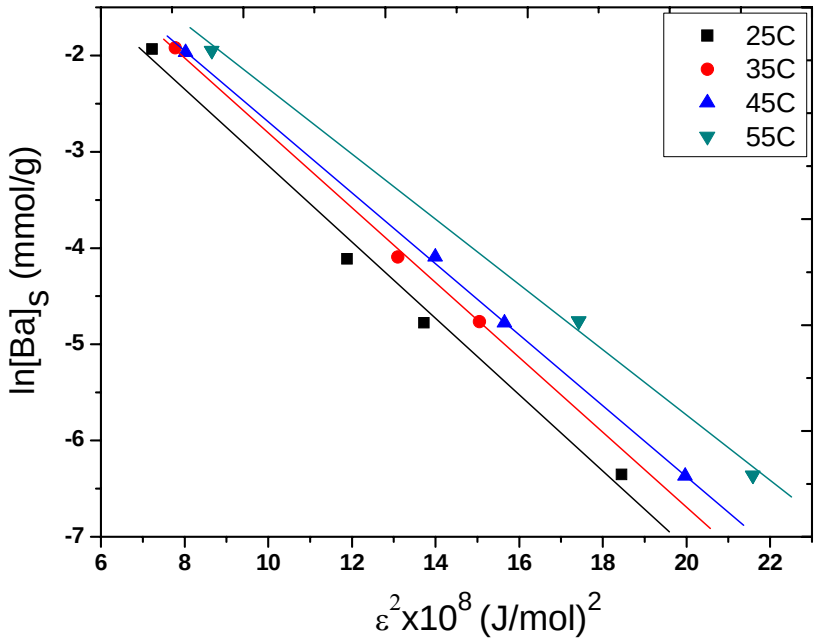

Fig. 3.24: Dubinin-Raduskevich isotherm plots for sorption of Ba^{2+} onto sodium form of insolubilized humic acid at various temperatures using 5 mg sorbent.

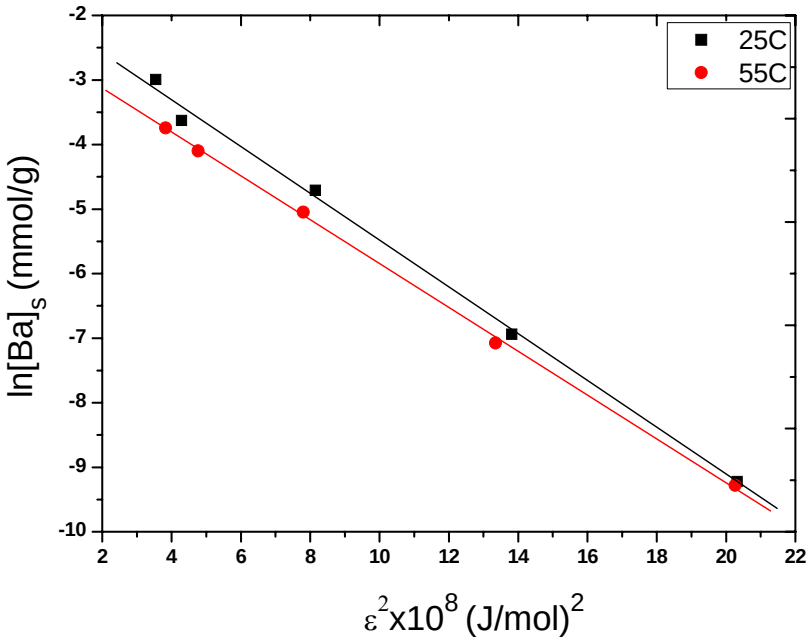

Fig.3.25: Dubinin-Raduskevich isotherm plots for sorption of Ba^{2+} onto iron nanoparticles at 25˚C and 55˚C using 100 mg sorbent.

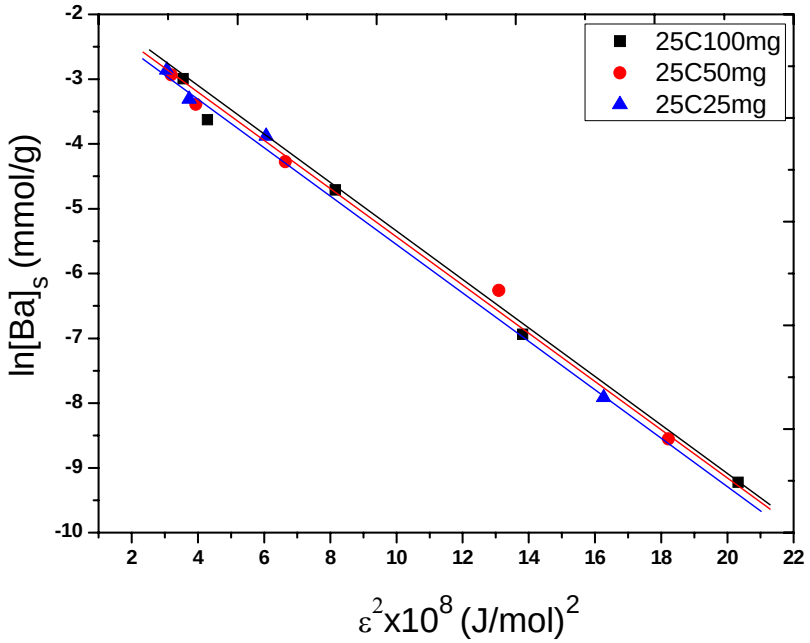

Fig. 3.26: Dubinin-Raduskevich isotherm plots for sorption of Ba^{2+} onto iron nanoparticles at 25˚C with different weights 25mg, 50mg and 100mg.

Table 3.12: The D-R Isotherm constants , K $(mol/kJ)^2$, C_m (mmol/100g) , and E (kj/mol) obtained from the least square fits for the sorption data of Cs^+ onto sodium form of insolubilized humic acid.
(The Linear Correlation Coefficients were all greater than 0,9915)

Sorbed Ion	D-R Constant	Temperature (K)			
		288	298	308	318
Cs^+	C_m	71,1	71,1	74,4	60,0
	K	$4,1 \times 10^{-3}$	$3,8 \times 10^{-3}$	$3,5 \times 10^{-3}$	$3,2 \times 10^{-3}$
	E	11,05	11,48	11,88	12,57

Table 3.13: The D-R Isotherm constants , K $(mol/kJ)^2$, C_m (mmol/100g) , and E (kj/mol) obtained from the least square fits for the sorption data of Ba^{2+} onto sodium form of insolubilized humic acid.
(The Linear Correlation Coefficients were all greater than 0,9973)

Sorbed Ion	D-R Constant	Temperature (K)			
		298	308	318	328
Ba^{2+}	C_m	349,2	310,0	276,4	276,1
	K	$4,4 \times 10^{-3}$	$3,9 \times 10^{-3}$	$3,7 \times 10^{-3}$	$3,4 \times 10^{-3}$
	E	10,61	11,26	11,64	12,16

Table 3.14: The D-R Isotherm constants , K $(mol/kJ)^2$, C_m (mmol/100g) , and E (kj/mol) obtained from the least square fits for the sorption data of Ba^{2+} onto iron nanoparticles.
(The Linear Correlation Coefficients were all greater than 0,9940)

Sorbed Ion	D-R Constant	Temperature (K)	
		298	328
Ba^{2+},100mg	C_m	15.7	8.515
	K	3.6×10^{-3}	3.4×10^{-3}
	E	11.73	12.15
Ba^{2+},50mg	C_m	15.8	
	K	3.6×10^{-3}	
	E	11.81	
Ba^{2+},25mg	C_m	17.7	
	K	3.8×10^{-3}	
	E	11.49	

3.2.2.5- Thermodynamic Results

The values of the thermodynamic parameters ΔHº, ΔSº and ΔGº of Cs^+ and Ba^{2+} sorption were obtained by fitting the experimental data to Arrhenius equations (13) and (14) given below. The graphs are shown in Figs. 3.27, 3.28 and 3.29 and the results are listed in Tables 3.15, 3.16 and 3.17.

$$\ln R_d = \frac{\Delta S^\circ}{R} - \frac{\Delta H^\circ}{RT} \qquad (13)$$

$$\Delta G^\circ = \Delta H^\circ - T\Delta S^\circ \qquad (14)$$

ΔHº and ΔSº values are dependent only on the temperature and pressure, therefore no concentration dependence is expected. Different R_d values are obtained at different loadings (initial concentrations of a particular cation). Therefore, distribution ratio, R_d, in equation (13) is an empirical equilibrium constant that is valid at a particular initial concentration and reaction conditions. This difficulty associated with the description of sorption data which is the lack of a thermodynamic equilibrium constant over a wide range of concentrations can be partially overcome by applying empirical distribution constants. In order to obtain values of these thermodynamic constants that are representative over the entire concentration ranges, averaged ΔHº and ΔSº values of different sorption cases were calculated. Consequently, an assumption is made in which the fluctuations in the ΔHº and ΔSº values are small enough to calculate the average of these values at different concentrations[35].

Enthalpy changes show the dependence of the sorption processes to the temperature. ΔHº values for Cs^+ and Ba^{2+} sorption onto INaA indicate that sorption behavior of Cs^+ onto INaA is an exothermic, and for Ba^{2+}, it is an endothermic process, but both values are close to zero which means that those processes are not significantly effected by the temperature change. In liquid-solid systems, when temperature is increased, the behavior of ions in solution or on the solid will be subject to factors such as the interionic forces, the hydration energy, the availability of sorption sites and the relative stability of sorbed ions at these sites[36]. Exothermic

behavior of Cs^+ ion sorption onto INaA and Ba^{2+} sorption onto iron nanoparticles can explained by thermal destabilization leading to an increase of the mobility of the Cs^+ and Ba^{2+} on the surface of the solid as the operating temperature is increased. In the literature[37], it is reported that the parallel increase in the Cs^+ ion mobility within the solution - which could make a positive contribution to sorption - is expected to be insignificant because Cs^+ ion already have a high mobility due to the weak hydration forces of water molecules which is caused by the low charge density (charge/size) of Cs^+ ions. Positive ΔH^o value was obtained for Ba^{2+} sorption onto INaA. There is a large difference in hydration enthalpies[38], being -276 kj/mol for Cs^+ and -1305 kj/mol for Ba^{2+} ions. In the literature[39], it is reported that metal ions with high hydration energies are well solvated in water and for cations that are solvated well in water, sorption requires that such ions should be stripped out to a certain extent of their hydration shell which is a process that requires energy input. If this deydration energy exceeds the exothermicity associated with the sorption of a metal ion on a solid, then the overall energy balance will lead to an endothermic behavior. If we formulate this phenomenon, sorption enthalpy (observed enthalpy change, ΔH^o_{obs}) includes the contributions of both intrinsic enthalpy change, ΔH^o_{int}, and the hydration enthalpy of the sorbate cation, ΔH^o_{hyd}. These enthalpies are related through the relation[40].

$$\Delta H^o_{obs} = \Delta H^o_{int} - \Delta H^o_{hyd}. \qquad (15)$$

The difference between ΔH^o values of Ba^{2+} sorption onto iron nanoparticles and Cs^+ and Ba^{2+} onto INaA can be understood by the hydration energy concept. The hydrated radius of ions determines the mobility of ions in solution to some extent and as the hydrated radius increases, the mobility and interaction ability decreases. Humic acid has a complex structure and sorption process does not only take place on the surface, in this case ions also migrate into the structure and their accessibility inside the structure is not as easy as to the surface. In the case of iron nanoparticles, ions only adsorb to the surface. Therefore, hydration shell of cations -which would be sorbed to the INaA surface- should be dehydrated to some extent and this process requires more energy which explains higher sorption enthalpy

values of ions when INaA was used as a sorbent. In all sorption cases, ΔH^{o} values indicate the physical nature of the sorption process which correspond to weak electrostatic attractions.

In cases of Cs^{+} and Ba^{2+} sorption on INaA , positive ΔS^{o} values were obtained which showed that more disorder was generated in the system. However, the positive values of entropy change indicate that more mobility is generated within the system as a result of the sorption process. Generally, it is expected that the entropy change of the system should be negative at the end of the sorption reaction due to transferring the sorbate ions from a disordered state in solution to a more ordered state when fixed by sorbent. However, there are some other factors which should be considered. One of them is the dehydration steps that increase the mobility of ions and that of the surrounding water molecules in solution and also the release of bound sodium ions from solid phase to the liquid phase is another reason, generating more disordered state. It was also found that ΔS^{o} value of Ba^{2+} sorption onto INaA is approximately two times more than Cs^{+}. In the literature[41], it's reported that the positive values of ΔS^{o} resulting from sorption of divalent cations (Ba^{2+} in this case) on solid surfaces might suggest that ions displaced from the solid surface are greater in number than the sorbed Ba^{2+} ions, which means that two monovalent ions (Na^{+} in this case) may be exchanged for a single Ba^{2+} ion.

The calculated negative values of ΔG^{o} for all cases indicate that the sorption process of each is spontaneous and preferentially driven towards the products. Temperature change has no significant effect on ΔG^{o} values in all sorption cases.

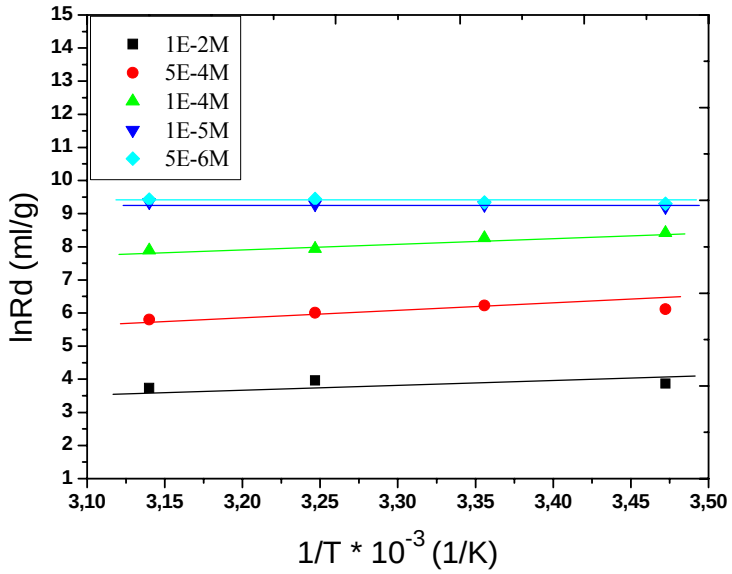

Fig. 3.27: Arrhenius plots for sorption of Cs^{+} onto sodium form of insolubilized humic acid

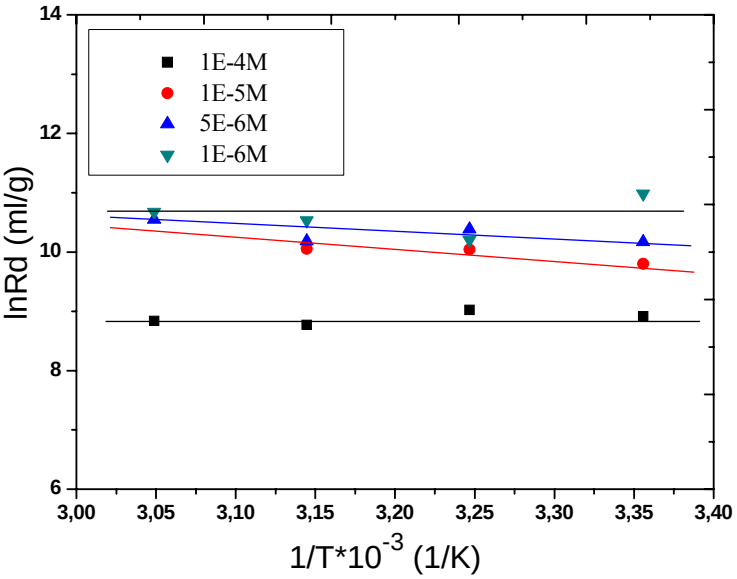

Fig. 3.28: Arrhenius plots for sorption of Ba^{2+} onto sodium form of insolubilized humic acid

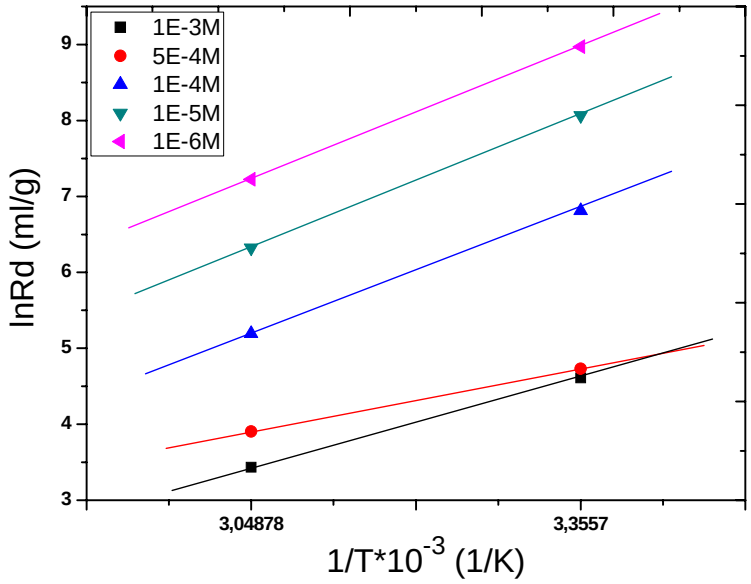

Fig. 3.29: Arrhenius plots for Sorption of Ba^{2+} onto iron nanoparticles

Table 3.15 : The average values of the enthalpy change, ΔH°_{av} (kJ/mol), entropy change, ΔS°_{av} (J/mol.K) and the calculated values of the Gibbs Free Energy change, ΔG° (kJ/mol), obtained at different temperatures for the sorption case of Cs^{+} onto sodium form of insolubilized humic acid.

Sorbed Ion	**ΔH°_{av} (kJ/mol)**	**ΔS°_{av} (J/mol.K)**	**ΔG° (kJ/mol) at Different Temperatures (K)**			
			288	**298**	**308**	**318**
Cs^{+}	-3.673	48.85	-17.74	-18.23	-18.72	-19.21

Table 3.16 : The average values of the enthalpy change, ΔH°_{av} (kJ/mol), entropy change, ΔS°_{av} (J/mol.K) and the calculated values of the Gibbs Free Energy change, ΔG° (kJ/mol), obtained at different temperatures for the sorption case of Ba^{2+} onto sodium form of insolubilized humic acid.

Sorbed Ion	**ΔH°_{av} (kJ/mol)**	**ΔS°_{av} (J/mol.K)**	**ΔG° (kJ/mol) at Different Temperatures (K)**			
			298	**308**	**318**	**328**
Ba^{2+}	2.102	89.522	-24.575	-25.470	-26.366	-27.261

Table 3.17: The average values of the enthalpy change, ΔH°_{av} (kJ/mol), entropy change, ΔS°_{av} (J/mol.K) and the calculated values of the Gibbs Free Energy change, ΔG° (kJ/mol), obtained at different temperatures for the sorption case of Ba^{2+} onto iron nanoparticles.

Sorbed Ion	**ΔH°_{av} (kJ/mol)**	**ΔS°_{av} (J/mol.K)**	**ΔG° (kJ/mol) at Different Temperatures (K)**	
			298	**328**
Ba^{2+}	-38.5	-73.98	-16.45	-14.23

3.2.3- Effect of surfactant modification upon phenol and cation sorption affinity

3.2.3.1- Sorption studies using UV-VIS spectroscopy

3.2.3.1.1- Kinetic Studies

Phenol is an extremely harmful organic contaminant for which an intense research effort is being made to develop methods to remove it from environment. Phenol is an aromatic compound and its availability in solutions can be monitored by using a UV-Visible spectrophotometer which gives two broad bands with λ_{max} values 211 and 270 nm in water.

In our experiment we tried to remove phenol from an aqueous solution onto a solid phase by using INaA (sodium form of insolubilized humic acid) as a sorbent. The results showed that phenol was not sorbed by INaA significantly, because negatively charged surface of INaA did not allow the sorption of polar phenol molecules. Therefore, surface of INaA was modified by using a cationic surfactant (cetyltrimethylammoniumchloride) so that negatively charged surface were neutralized by cationic part of surfactant and phenol molecules were able to interact with highly hydrophobic (nonpolar) tails of surfactant molecules. It was found that cationic part of surfactant and negatively charged surface of INaA interacted strongly and alkyl peaks appeared at 2928 and 2857 cm^{-1} as shown in Fig. 3.5.

To understand the kinetic behavior and determine the equilibrium time for phenol sorption onto surfactant modified insolubilized humic acid (SMIA), absorbance values of the remaining phenol in solution were measured at different shaking times ranging from 1 hour to 72 hours. The significant decrease at the absorbance values with time can easily be seen from the absorbance spectra of phenol solutions as shown in Fig. 3.30 and data in Table 3.18. These indicate the adsorption of phenol molecules onto the solid phase. Equilibrium time of phenol removal was found to be 48 hours and remained nearly constant thereafter as shown in Fig. 3.31. Phenol sorption was found to obey to the pseudo second order rate law quite well Eq. (6,7) as shown in Fig. 3.32. Kinetic data is given in Table 3.19.

The equilibrium time for phenol sorption onto SMIA is more than the equilibrium time for cation sorptions onto INaA and iron nanoparticles. Surface properties of INaA underwent modifications and changed significantly. The interactions between surfactant molecules and phenol molecules are relatively weak, compared to interactions between cations and negatively charged INaA surface. This would delay the equilibrium time for the sorption of phenol molecules onto SMIA. The other factor for the longer equilibrium time can be attributed to the molecular size of phenol which is much larger than the hydrated size of cations. This lowers the mobility of phenol molecules as a result more time is required for equilibration.

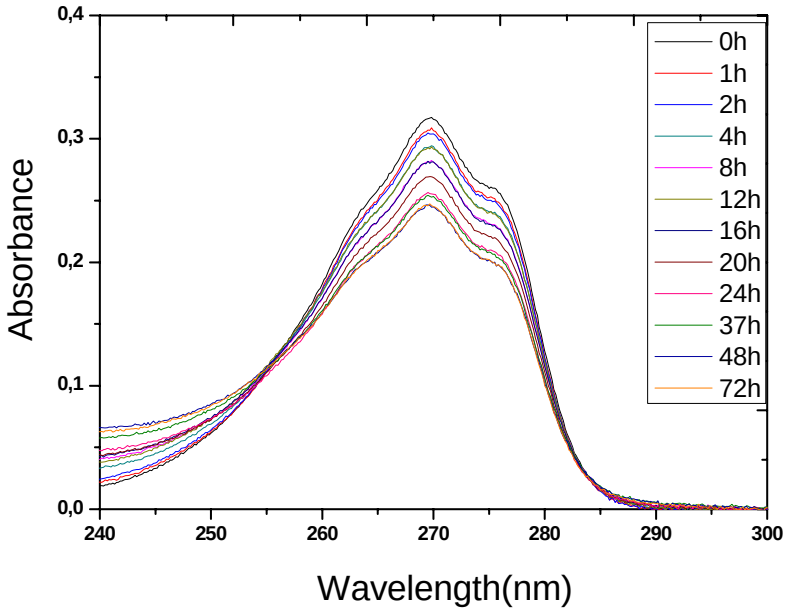

Fig. 3.30: UV-Vis absorption spectra of phenol solutions remaining in solution after sorption at different shaking times

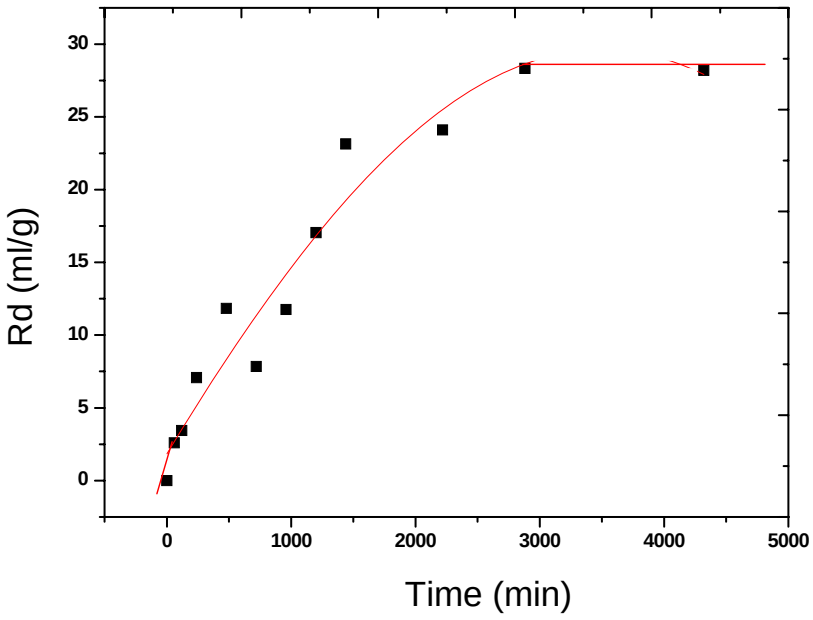

Fig. 3.31: Variation of R_d values with shaking time for phenol sorption onto surfactant modified insolubilized humic acid at 25°C

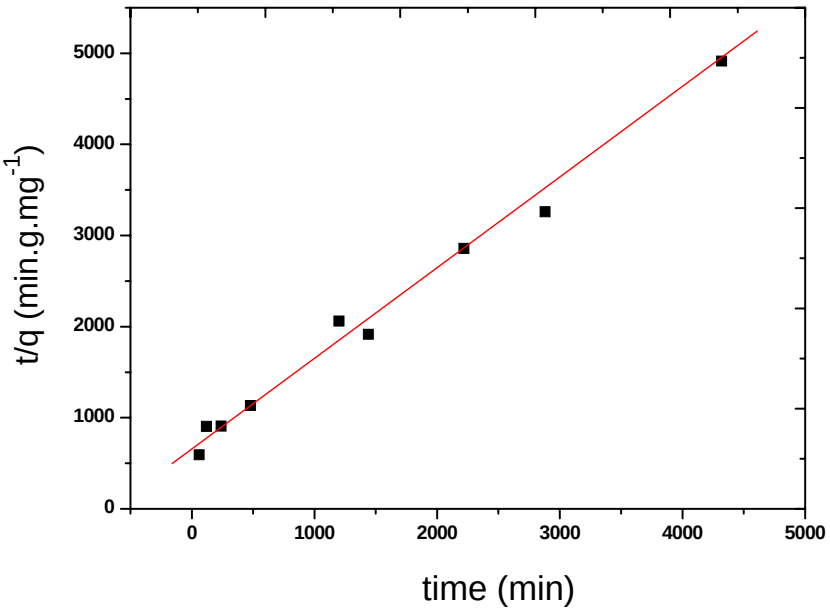

Fig. 3.32: Variation of t/q Values with Shaking time for Ba^{2+} sorption onto surfactant modified insolubilized humic acid at 25°C

Table 3.18 : The kinetic data of phenol sorption onto surfactant modified insolubilized humic acid at different times at 25ºC

Time (min)	Absorbance	$[Phenol]_s$ (mg/g)	$[Phenol]_{liq}$ (mg/L)	Rd (ml/g)
0	0,31578	0	20	0
60	0,30662	0,101	19,49	5,18
120	0,30412	0,133	19,34	6,86
240	0,29372	0,264	18,68	14,15
480	0,28116	0,423	17,88	23,67
720	0,29164	0,290	18,55	15,67
960	0,28135	0,421	17,90	23,52
1200	0,26857	0,583	17,09	34,10
1440	0,25520	0,752	16,24	46,30
2220	0,25324	0,777	16,12	48,19
2880	0,24483	0,883	15,58	56,67
4320	0,24512	0,879	15,60	56,37
A 270nm				

Table 3.19 : Amount of sorbed phenol per gram of sorbent, pseudo second order rate constant and correlation coefficient value for phenol sorption.

Sorbent	Sorbed Substance	q_e (mg/g)	k_2 ($g.mg^{-1}.min^{-1}$)	R^2
SMIA	Phenol	1.04	$1.367x10^{-3}$	0.99

3.2.3.1.2- Freundlich and Tempkin isotherms for phenol sorption

The Freundlich (Eq.8) and Tempkin (Eq.17) isotherms described well the phenol sorption onto SMIA as shown in Figs 3.33 and 3.34, respectively. The data of sorption is given in Table 3.22. The Freundlich constants "n" and "k" obtained at 25ºC are listed in Table 3.20. The Freundlich constant "n" gives information about surface heterogeneity. Since the linearity of sorption increases as "n" approaches unity, SMIA shows a very high affinity for phenol molecules. Sorption affinity "k" values of phenol sorption onto SMIA are higher than the sorption affinity values of phenol sorption onto surfactant modified natural zeolites studied in the literature[44] under the same conditions.

Tempkin isotherm includes the effects of some indirect adsorbate/adsorbate interactions on adsorption isotherms and suggested that because of these interactions the heat of adsorption of all the molecules in the layer would decrease linearly with coverage.

The Tempkin isotherm has been used in the following form:

$$[Ph]_s = \frac{RT}{b} (\ln K [Ph]_l) \qquad (16)$$

Equation (16) can be expressed in its linear form as ;

$$[Ph]_s = B \ln K + B \ln[Ph]_l \qquad (17)$$

where

$$B = \frac{RT}{b} \qquad (18)$$

The adsorption data can be analyzed according to Eq. (17). A plot of $[Ph]_s$ (amount of phenol adsorbed onto SMIA at equilibrium, mg/g) versus $\ln[Ph]_l$ (the concentration of phenol in solution at equilibrium, mmol/ml) enables the determination of the constants "K", "B" and "b". The constant "B" is related to the

heat of adsorption[43]. "K" is the equilibrium binding constant (l/mg) corresponding to the maximum binding energy and "b" is the heat of adsorption. The Tempkin isotherm constants are listed in Table 3.21. The positive heat of adsorption shows that the sorption process exhibits endothermic behavior. The equilibrium constant value corresponds to negative Gibbs Free Energy change, ΔG^{o}, therefore sorption process is spontaneous and favors the products.

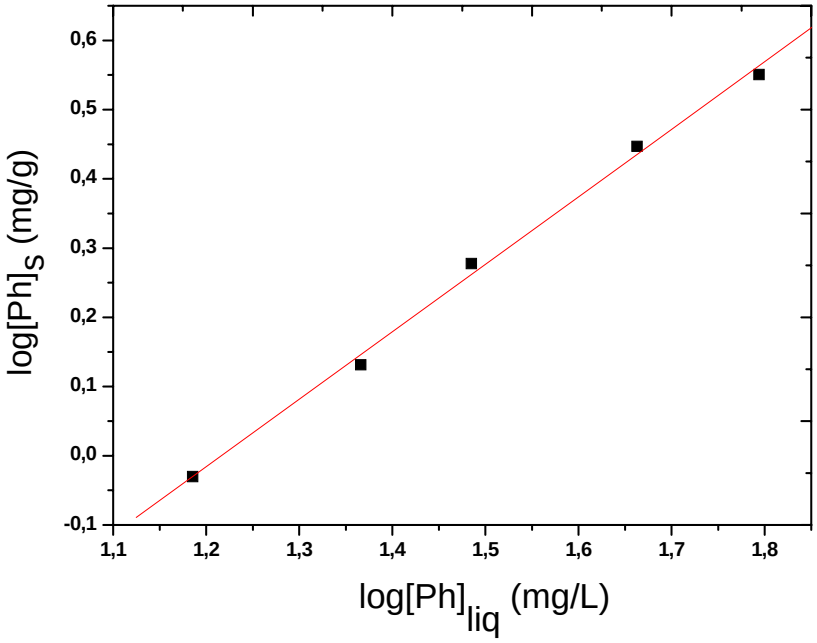

Fig. 3.33: Freundlich Isotherm plot for sorption of phenol onto surfactant modified insolubilized humic acid at 25˚C

Table 3.20 : Freundlich constants , n and k , obtained from the least square fits of the sorption data of phenol onto surfactant modified insolubilized humic acid.
(The Linear Correlation Coefficient is greater than 0,9965)

Sorbed Organic	**Freundlich Constant**	**Temperature (K)**
		298
Phenol	**n**	0.9746
	k	0.0653

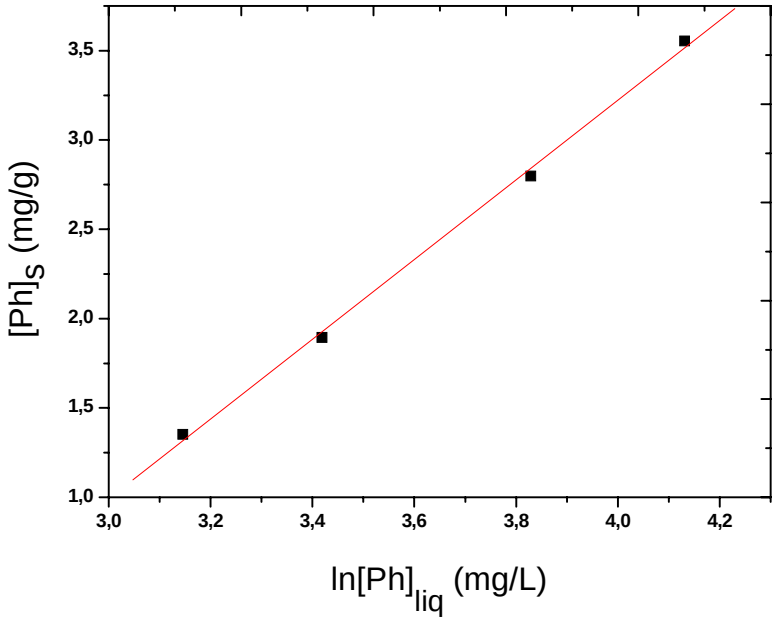

Fig. 3.34: Tempkin isotherm plot for sorption of phenol onto surfactant modified insolubilized humic acid at 25˚C

Table 3.21 : Tempkin isotherm constants , K(L/mg), B and b (kJ/mol) obtained from the least square fits of the sorption data of phenol onto surfactant modified insolubilized humic acid.

(The Linear Correlation Coefficient is greater than 0.998)

Sorbed Organic	**Tempkin Constant**	**Temperature (K)**
		298
Phenol	**K**	0.0776
	B	2.2316
	b	1.110

Table 3.22: The data of phenol sorption onto surfactant modified insolubilized humic acid at 25ºC and initial concentrations.

Temperature (K)	**[C]° (mg/L)**	**R_d (ml/g)**	**$[Ph]_s$ (mg/g)**	**$[Ph]_{liq}$ (mg/L)**
298	20	60,89	0,93	15,33
298	30	58,22	1,35	23,24
298	40	62,04	1,89	30,53
298	60	60,83	2,80	46,01
298	80	57,10	3,55	62,23

3.2.3.2- Sorption studies of cesium onto surfactant modified insolubilized humic acid

Loading experiment was carried out to find the number of adsorption sites responsible for cesium sorption onto SMIA as shown in Fig. 3.35. The shape of loading curve is similar to the loading curves of barium and cesium sorption onto INaA. The detailed analyses for similar loading curves were made in part (3.2.2.1). This loading curve indicates that the sorption occurs on single sorption site, as well. In this case, the responsible sorption site is again the negatively charged surface functional groups which are formed during the insolubilization process. Dubinin-Radushkevich isotherm described well the sorption data of cesium sorption onto SMIA as shown in Fig. 3.36 and Table 3.23. The cation exchange capacity (C_m) for cesium sorption onto SMIA is 2.5 times less than the C_m value for cesium sorption onto INaA (Table 3.12). Surfactant molecules occupied most of the negatively charged functional groups on INaA, therefore C_m value decreased in the case of cesium sorption onto SMIA. Adsorption mean free energy value (Table 3.23) indicates that sorption process is an ion-exchange type of sorption[35]. The exchanged ions are sodium ions remaining on the surface after surfactant modification.

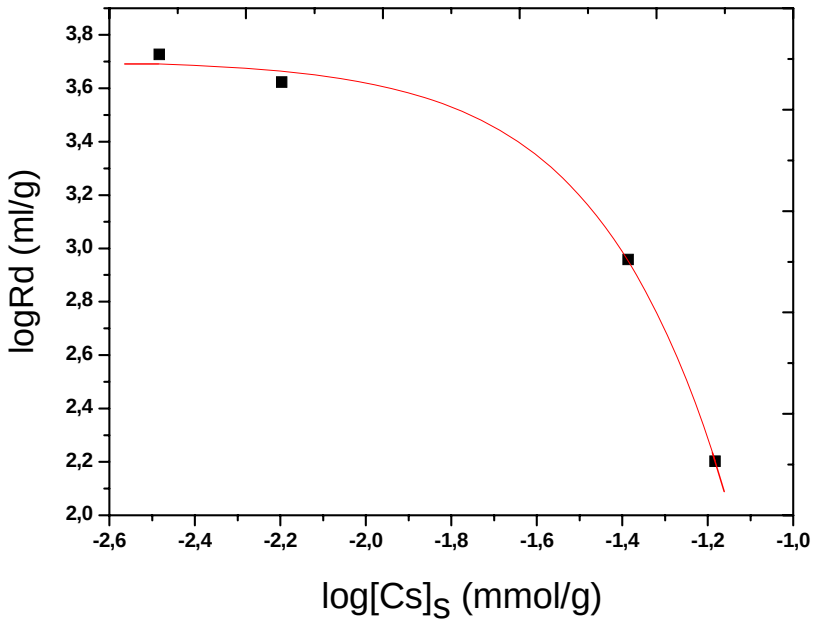

Fig. 3.35: The loading curve for sorption of Cs^+ onto surfactant modified insolubilized humic acid at 25ºC

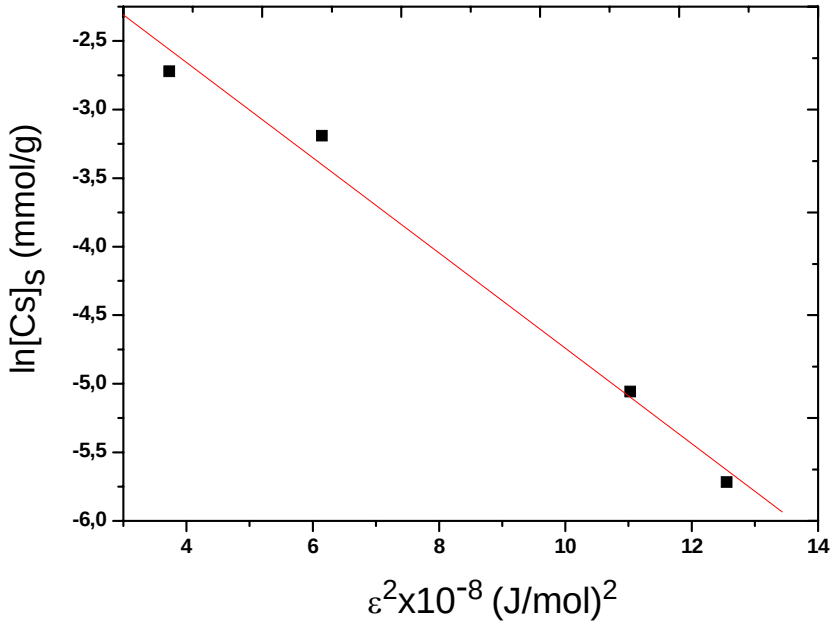

Fig. 3.36: Dubinin-Raduskevich isotherm plot for sorption of Cs^+ onto surfactant modified insolubilized humic acid at 25˚C

Table 3.23 : The D-R Isotherm constants, K $(mol/kJ)^2$, C_m (mmol/100g), and E (kj/mol) obtained from the least square fits for the sorption data of Cs^+ on surfactant modified insolubilized humic acid.
(The Linear Correlation Coefficient is greater than 0.9872)

Sorbed Ion	**D-R Constant**	**Temperature (K)**
		298
Cs^+	**C_m**	28.134
	K	$3.473x10^{-3}$
	E	12.0

The Freundlich isotherm also describes well the sorption data of cesium sorption onto SMIA (Fig. 3.37). The Freundlich constants "n" and "k" obtained at 25ºC are listed in Table 3.24. The results are similar with the "n" and "k" values obtained in the case of cesium sorption onto INaA. This shows that surfactant modification does not make a significant change on the sorption energy barrier and linearity of cesium sorption. The decrease upon the uptake of cesium ions is only the result of the decreasing number of negatively charged surface functional groups.

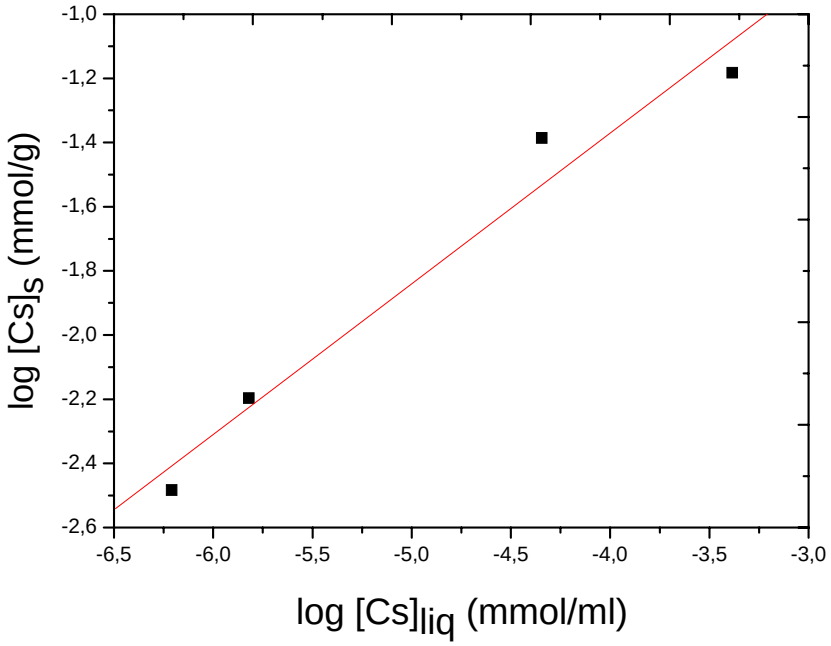

Fig. 3.37: Freundlich isotherm plots for sorption of Cs^+ onto surfactant modified insolubilized humic acid at 25˚C

Table 3.24 : Freundlich constants , n and k , obtained from the least square fits of the sorption data of Cs^+ onto surfactant modified insolubilized humic acid.

Sorbed Cation	**Freundlich Constant**	**Temperature (K)**
Cs^+	**n**	0.4695
	k	3.217

4. CONCLUSION

The results of this study may be summarized as:

- Insolubilized humic acid can be used as an effective adsorbent to remove radionuclides from aquatic environments. It does not have a tendency to sorb phenolic compounds, but its modification with cationic surfactants made it a good sorbent to remove phenolic compounds. Iron nanoparticles and surfactant modified insolubilized humic acid are also able to remove radionuclides, but they are not as effective adsorbent as insolubilized humic acid.

- Equilibrium in cation sorption is achieved within hours of contact between the solution of adsorbed cations and both humic acid and iron nanoparticle samples indicating that fast sorption mechanisms are involved and the sorption process is mainly a surface phenomena. In the case of phenol sorption onto surfactant modified insolubilized humic acid, equilibrium is achieved within 48 hours.

- Structural changes were determined using FTIR and ^{13}C NMR techniques during modification of humic acid. The amount of acidic functional groups (carboxylic and phenolic groups) decreased during insolubilization step, and cationic surfactant interacted well with surface of insolubilized humic acid. The responsible adsorption sites in iron nanoparticles and particle shape were determined using PXRD and SEM techniques, respectively. The cations are sorbed by the iron oxide surface and iron nanoparticles form aggregates.

- Kinetic studies indicated that adsorption behaviors of both cations and phenol obey the pseudo second order rate law. Cation sorption data have been interpreted in terms of Freundlich and Dubinin- Radushkevich equations. Phenol sorption data was described well by both Tempkin and Freundlich isotherms. There is an inverse

relationship between the rate of sorption and the sorption order for the cation sorptions studied.

- The pH experiments showed that insolubilized humic acid has a higher sorption capacity towards cations at high pH values, because of the dissociation of all acidic hydrogens.

- The sorption data obtained at different temperatures indicate that cation sorption onto insolubilized humic acid is not affected significantly by the temperature change whereas cation sorption onto iron nanoparticles is an exothermic process. Positive entropy values were found in the case of cation sorption onto insolubilized humic acid whereas negative entropy values were calculated upon cation sorption onto iron nanoparticles. Negative ΔG^{o} values in all cation sorption processes show that sorption process is spontaneous.

REFERENCES

[1] Manahan, S.E., Fundamentals of Environmental Chemistry, Lewis publishers, pp. 406-410, 721-746 (2001)

[2] Kaushik, C.P., Mishra, R.K., Sengupta, P., Amar Kumar, Das, D., Kale, G.B., Kanwar Raj Barium Borosilicate Glass – a Potential Matrix for Immobilization of Sulfate Bearing High-Level Radioactive Liquid Waste. J. Nucl. Mater., 358, 129–138 (2006)

[3] Ebner, A.D., Ritter, J.A, Navratil, J.D. Adsorption of Cesium, Strontium, and Cobalt Ions on Magnetite and a Magnetite-Silica Composite. Ind. Eng. Chem. Res., 40, 1615- 1623 (2001)

[4] Shahwan, T. M.Sc. Thesis. Bilkent University, Department of Chemistry (1997)

[5] Girelli, A.M., Mattei,E., Messina, A. Phenols Removal by Immobilized Tyrosinase Reactor in On-Line High Performance Liquid Chromatography. Anal. Chim. Acta, 580, 271-277 (2006)

[6] Senel, S., Kara, A., Alsancak, G., Denizli, A., Removal of Phenol and Chlorophenols from Water with Reusable Dye-Affinity Hollow Fibers. J. Hazard. Mater., B138, 317-325 (2006)

[7] Assemi, S., M.Sc. Thesis. Bilkent University (1992)

[8] Tan, K.H., Principles of Soil Chemistry, Marcel Dekker (1998)

[9] Vertes, A., Nagy, S., Klencsar, Z., Molnar, G.L., Handbook of Nuclear Chemistry, volume 3, Chemical Applications of Nuclear Reactions and Radiations, Kluwer Academic Publishers, pp. 443-444 (2003)

[10] http://en.wikipedia.org/wiki/Gamma_spectroscopy

[11] http://en.wikipedia.org/wiki/UV/VIS_spectroscopy

[12] Steelink, C., Investigating Humic Acids in Soils. Anal. Chem. A-Pages, 74, 326A-333A (2002)

[13] Sutton, R., Sposito, G., Molecular Structure in Soil Humic Substances: The New View. Environ. Sci. Technol., 39, 9009-9015 (2005)

[14] Simpson, A.J., Kingery, W.L., Hayes, M.H.B, Molecular Structures and Associations of Humic Substances in the Terrestrial Environment Naturwissenschaften, 89, 84-88, (2002)

[15] Gezici, O., Kara, H., Ersöz, M., Abali, Y., The Sorption Behavior of a Nickel-Insolubilized Humic Acid System in a Column Arrangement. J. Colloid Interface Sci., 292, 381-391 (2005)

[16] Seki, H., Suzuki, A., Adsorption of Heavy Metal Ions onto Insolubilized Humic Acid J. Colloid Interface Sci., 171, 490-494 (1995)

[17] Yee, M.M., Miyajima, T., Takisawa, N., Evaluation of Amphiphilic Properties of Fulvic Acid and Humic Acid by Alkylpyridinium Binding Study. Colloid and Surfaces A: Physicochem. Eng. Aspects, 272, 182-188 (2006)

[18] Nurmi, J.T, Tratnyek, P.G., Sarathy, V. Characterization and Properties of Metallic Iron Nanoparticles: Spectroscopy, Electrochemistry, and Kinetics. Environ. Sci. Technol., 39, 1221-1230 (2005)

[19] Li, X., Zhang, W. Iron Nanoparticles: the Core-Shell Structure and Unique Properties for Ni(II) Sequestration. Langmuir, 22, 4638-4642 (2006)

[20] Shahwan, T., Erten, H.N. Temperature Effects in Barium Sorption on Natural Kaolinite and Chlorite-Illite Clays J. Radioanal. Nucl. Chem., 260, 43-48 (2004)

[21] Shahwan, T., Erten, H.N. Thermodynamic parameters of Cs^+ sorption on natural clays J. Radioanal. Nucl. Chem., 253, 115–120 (2002)

[22] Gran, G., Determination of the Equivalence Point in Potentiometric Titrations Analyst, 77, 661-671 (1952)

[23] Benites, V.M, Mendonca, E., Schaefer, C.E.G.R., Novotny, E. H., Reis, E.L., Ker, J. C. Properties of black soil humic acids from high altitude rocky complexes in Brazil Geoderma , 127, 104–113 (2005)

[24] Shirshova, L. T. , Ghabbour, E. A., Davies, G. Spectroscopic characterization of humic acid fractions isolated from soil using different extraction procedures Geoderma, 133, 204– 216 (2006)

[25] Xu, D. , Zhu, S. , Chen, H. , Li, F. Structural characterization of humic acids isolated from typical soils in China and their adsorption characteristics to phenanthrene Colloids and Surfaces A: Physicochem. Eng. Aspects, 276, 1–7 (2006)

[26] Simpson, M.J., Simpson, A.J., Hatcher, P.G. Non-covalent associations between hydrophobic organic contaminants and dissolved organic material observed by NMR Environ. Toxicol. Chem., 23(2), 355-362 (2004)

[27] Cook, R.L., Langford, C. Structural Characterization of a Fulvic Acid and a Humic Acid Using Solid-State Ramp-CP-MAS ^{13}C Nuclear Magnetic Resonance Environ. Sci. Technol., 32, 719-725 (1998)

[28] Frund, R., Ludemann, H.D., Gonzalez-Vila, F.J. , Almendros, G., del Rio, J.C., Martin, F. Structural differences between humic fractions from different soil types as determined by FT-IR and 13 C-NMR studies Sci. Total Environ., 81/82, 187-194 (1989)

[29] Lien, H., Jhuo, Y., Chen, L. Effect of Heavy Metals on Dechlorination of Carbon Tetrachloride by Iron Nanoparticles Environ. Eng. Sci., 24, 21-30 (2007)

[30] Sohn, K., Kang, S.W., Ahn, S., Woo, M., Yang, S. Fe (0) Nanoparticles for Nitrate Reduction: Stability, Reactivity, and Transformation Environ. Sci. Technol., 40, 5514-5519 (2006)

[31] Shahwan, T., Suzer, S., Erten, H.N. Sorption Studies of Cs^+ and Ba^{2+} Cations on Magnesite. Appl. Radiat. Isot. 49, 915-921 (1998)

[32] Azizian, S. Kinetic models of sorption: a theoretical analysis J. Colloid Interface Sci., 276, 47-52 (2004)

[33] Bohn, H.L., McNeal, B.L., and O'Conner, G.A., Soil Chemistry, John Wiley and Sons, New York, pp. 341 (1985)

[34] Helferrich, F. Ion Exchange, McGraw Hill (1962)

[35] Shahwan, T. Ph.D. Thesis. Bilkent University, Department of Chemistry (2000)

[36] Shahwan, T., Erten, H.N., Unugur, S. A characterization study of some aspects of the adsorption of aqueous Co^{2+} ions on a natural bentonite clay J. Colloid Interface Sci., 300, 447–452 (2006)

[37] Shahwan, T., Akar, D., Eroğlu, A.E. Physicochemical characterization of the retardation of aqueous Cs^+ ions by natural kaolinite and clinoptilolite minerals J. Colloid Interface Sci. 285, 9–17 (2005)

[38] http://www.science.uwaterloo.ca/~cchieh/cact/applychem/hydration.html

[39] Akar, D., Shahwan, T., Eroglu, A.E. Kinetic and Thermodynamic Investigations of Strontium Ions Retention by Natural Kaolinite and Clinoptilolite Minerals Radiochim. Acta 93, 477-485 (2005)

[40] Li, H., Teppen, B.J., Johnston , C., Boyd, S. Thermodynamics of Nitroaromatic Compound Adsorption from Water by Smectite Clay Environ. Sci. Technol. 38, 5433-5442 (2004)

[41] Khan, S.A., Reman, R.U., Khan, M.A. Adsorption of Cs(I), Sr(II) and Co(II) on Al_2O_3 J. Radioanal. Nucl. Chem. 190, 81-96 (1995)

[42] Masini, J.C, Abate, G., Lima, E.C., Hahn, L.C, Nakamura, M.S., Lichtig, J., Nagatomy, H.R. Anal. Chim. Acta, 364, 223-233 (1998)

[43] Allen, S.J, Mckay, G., Porter, J.F. Adsorption isotherm models for basic dye adsorption by peat in single and binary component systems J. Colloid Interface Sci., 280, 322–333 (2004)

[44] Kuleyin, A., Removal of phenol and 4-chlorophenol by surfactant-modified natural zeolite J. Hazard. Mater. (2006), doi:10.1016/j.jhazmat.2006.10.036